Geochronology of the Whittlesey sedimentary succession, eastern England: The 'Pompeii' of the British late Middle Pleistocene to Holocene record

H. E. LANGFORD,[1]* [iD] M. D. BATEMAN,[2] R. M. BRIANT[1] [iD] and D. J. HORNE[3,4]
[1]School of Social Sciences, Birkbeck University of London, London, UK
[2]School of Geography and Planning, University of Sheffield, Sheffield, UK
[3]School of Geography, Queen Mary, University of London, London, UK
[4]Department of Earth Sciences, The Natural History Museum, London, UK

ABSTRACT: The sedimentary succession at Whittlesey preserves a unique British late Middle Pleistocene to Holocene record back to a time equivalent to at least marine oxygen isotope stage 8 (ca. 250 ka). This study builds on previously published sedimentology, geochronology and palaeoecology results to establish 20 sedimentary facies associations, with 14 of them dated by luminescence, amino acid geochronology or radiocarbon age-estimate techniques. This remarkable fluvial archive provides insight into the past three glacial–interglacial cycles for eastern England and is ideally located geographically to inform reconstructions of past ice limits, sea level, temperature and drainage networks affecting the North Sea and Fenland. This robust chronostratigraphic framework provides a reference against which to assess previous work in the region and highlights future research directions.
© 2025 The Author(s). *Journal of Quaternary Science* Published by John Wiley & Sons Ltd.

KEYWORDS: amino acid geochronology; depositional record; quaternary palaeoecology; radiocarbon and thermoluminescence dating; research framework; stratigraphical interpretation

INTRODUCTION

A recently found Bronze Age village has been dubbed 'Britain's Pompeii' (Knight et al., 2024), not only in terms of importance but also, as at Pompeii, because the remains are exceptionally well preserved and provide a unique, momentary insight into the daily life of its inhabitants. The sedimentary context of this archaeological treasure also preserves an exceptional British late Middle Pleistocene to Holocene record (Langford, 2002; Langford and Briant, 2004; Langford et al., 2004a, 2004b, 2004c, 2007; Smith et al., 2012; Briant et al., 2018) back to a time at least equivalent to marine oxygen isotope stage (MIS) 8 (ca. 250 ka; Lisiecki and Raymo, 2005; Railsback et al., 2015); it is also listed among the top 50 UK Quaternary sites (https://www.qra.org.uk/our-work/outreach/top-50-quaternary-sites/). As fossil-bearing Pleistocene deposits are uncommon, the sedimentary succession at Whittlesey, eastern England (Fig. 1), records unique insights into British Quaternary history. For example: (i) the only post-Hoxnian (Holsteinian/MIS 11) occurrence of the exotic mollusc *Theodoxus danubialis* (Langford et al., 2014a) and the only occurrence of this species outside the River Thames catchment; (ii) three distinctive post-Anglian (Elsterian/MIS 12) late Middle Pleistocene cool/cold stage fossil assemblages (Langford et al., 2014b); (iii) the early onset of the last interglacial (LIG) and the only fully fluvial Ipswichian (Eemian/MIS 5e) deposit so far recorded in the River Nene catchment (Langford et al., 2017); and (iv) evidence from marine-influenced sediments that provide insight into penultimate and LIG sea levels (Langford et al., in press). Here, we complement the archaeological reports

by providing a geological perspective on a site that, in terms of importance, could be considered the 'Pompeii' of the British late Middle Pleistocene to Holocene record.

As Bridgland (2010) notes, our knowledge of the complexity of the Quaternary Period is drawn mainly from deep-sea and ice cores, but these are necessarily global in scale and do not capture local detail, such as the significant asynchroneity in glacial conditions at a variety of scales (Gibbard and Hughes, 2021), for which terrestrial stratigraphic archives are important. The securely dated deposits of the Quaternary Whittlesey sedimentary succession (WSS) therefore provide important local information that is not available from deep-sea or ice cores.

Long-term records reported previously for English fluvial systems (e.g. Gibbard, 1985; Maddy et al., 1991; Bridgland, 1994; Howard et al., 2007; Bridgland et al., 2015) have tended to be coarse-resolution studies of fragmentary deposits. Historically, stratigraphical interpretation of such records has been based on long profiles established from the relative heights of fragmentary alluvial deposits (morphostratigraphy; Rose, 2009), supported by lithology and scattered age-estimate and biostratigraphic data (Lewis et al., 2021). More recently, comprehensive luminescence dating programmes have been applied (Briant et al., 2006; Brown et al., 2015; Hatch et al., 2017), occasionally in combination with amino-acid geochronology (AAG) dating (Briant et al., 2012). The adopted morphostratigraphy assumes downstepping fluvial sediment bodies where age increases with elevation (e.g. Maddy, 1999; Rose, 2015). Taylor (1963) and Horton (1989) have proposed such an aggradation pattern for the River Nene, but this approach has led to ambiguity and several alternative interpretations (Table 1). In contrast, the complex WSS

*Correspondence H. E. Langford, School of Social Sciences, as above.
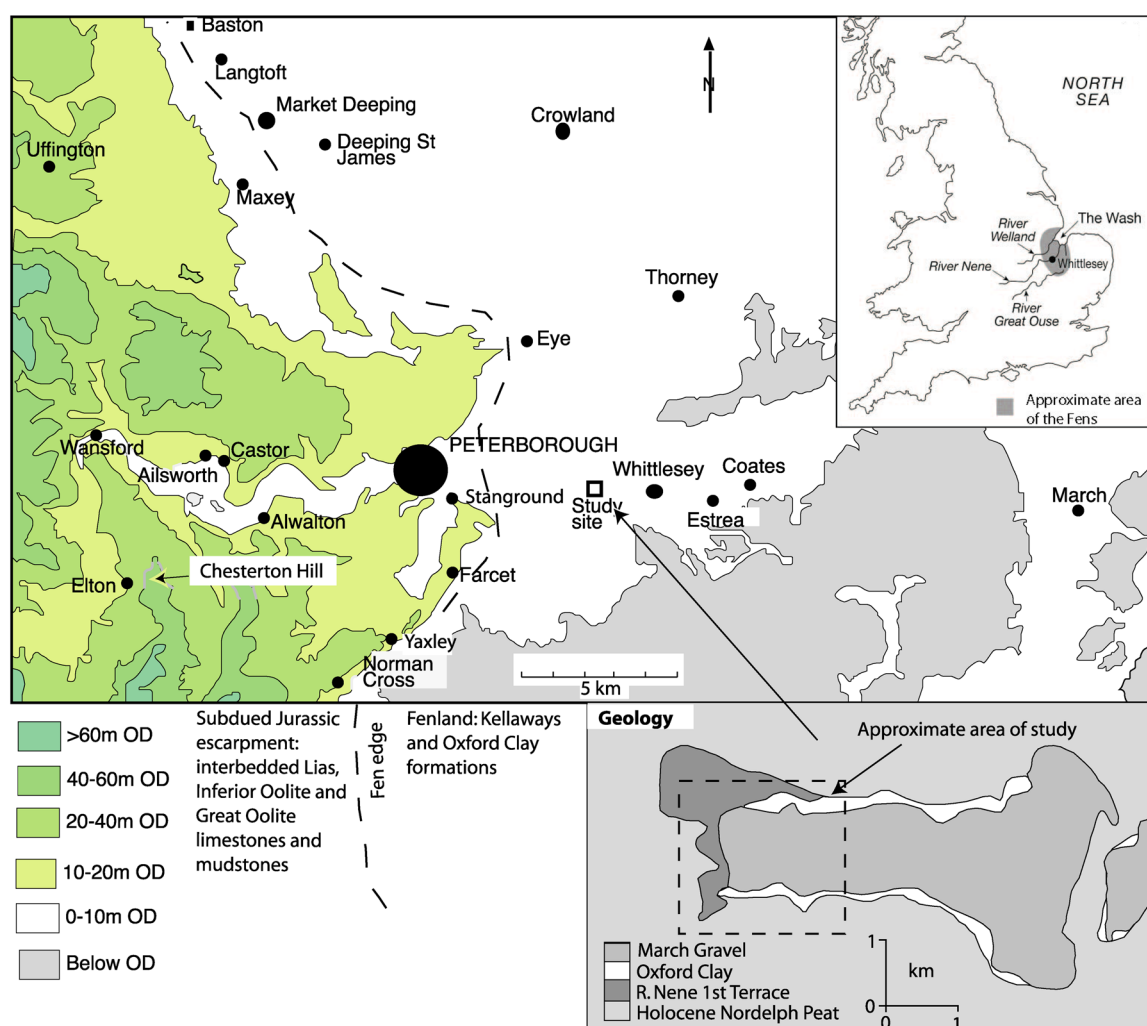Email: h.langford@bbk.ac.uk

Figure 1. Topography of the western edge of Fenland and location of the study site relative to the Jurassic escarpment. Inset: location of The Wash and the Fens in eastern England and the Great Ouse, Nene and Welland rivers that drain the Cambridgeshire Fens. Bottom right: geology of the study site. (Based on Langford, 1999.). [Color figure can be viewed at wileyonlinelibrary.com]

comprises juxtaposed packages of vertically stacked deposits, similar to those found elsewhere in the Nene catchment at Sutton Cross (Langford et al., 2020), 16 km upstream (Fig. 2). Such non-conformity with the expectations of the morphostratigraphy adopted is not uncommon (e.g. Green et al., 1996; West et al., 1999; Brown et al., 2015; Hatch et al., 2017).

Unravelling the stratigraphy of the complex WSS has required detailed sedimentology supported by palaeoecology, clast lithology, numerical age-estimates (^{14}C, AAG and luminescence) and biostratigraphy, with several studies seeking to clarify uncertain age relationships within the succession (Langford et al., 2007, 2014a, 2014b, 2017, in press; Briant et al., 2018). Recent accounts of River Nene Pleistocene deposits that adopt the traditional morphostratigraphy have not acknowledged this complexity (e.g. Rose, 2015; White et al., 2017), or have failed to understand the approach adopted to study such complexity (e.g. Westaway, 2009), or have questioned the findings of this research (Gibbard et al., 2018). There is therefore a clear need to demonstrate a comprehensive and rigorous chronostratigraphy for the WSS.

In addition to stratigraphical interpretation, fluvial sedimentary records combined with geomorphology provide a means for reconstructing drainage network evolution (Langford, 2018), knowledge of which is as fundamental to understanding British landscape history as is knowledge of Pleistocene ice advances and limits (Gibbard et al., 2012). As Whittlesey is located 6 km eastward of the fen edge (Figs. 1 and 2), the WSS has the potential to provide important information on Fenland Quaternary history (sensu Skertchly, 1877, Fowler, 1933; Macfayden, 1933; Godwin, 1940), critical for understanding the extent of late Middle to Late Pleistocene glaciations and post-Anglian drainage network evolution (Straw, 2000, 2011; Boreham et al., 2010; Westaway, 2010; White et al., 2010, 2017; Bridgland et al., 2015; Langford, 2018; Gibbard et al., 2021; Gibson et al., 2022). Such understanding could resolve contrasting views on post-Anglian evolution of Fenland and the differing interpretations of the Quaternary stratigraphy of the area (Table 1; Horton, 1989; Bridgland et al., 1991; Maddy, 1999; Boreham et al., 2010; Lee et al., 2015).

A primary aim of this study, as with earlier research, is to present new age estimates (AAG and luminescence) in order to improve stratigraphical understanding of the WSS (Table 2). A successful outcome, when combined with previous dating results, will lead to a robust chronostratigraphy for the WSS, thus providing a reliable Quaternary framework for present and future research. With this in mind, the integrated dating results are combined with the sedimentological and palaeoenvironmental data from previous studies to determine sedimentary facies associations (i.e. those major and minor lithofacies related to each other by depositional environment in space and time). This robustly dated WSS could then form the basis of a locally and regionally relevant formal or informal database/framework to be developed over time in order to build a definitive Quaternary history of Fenland, and thus a
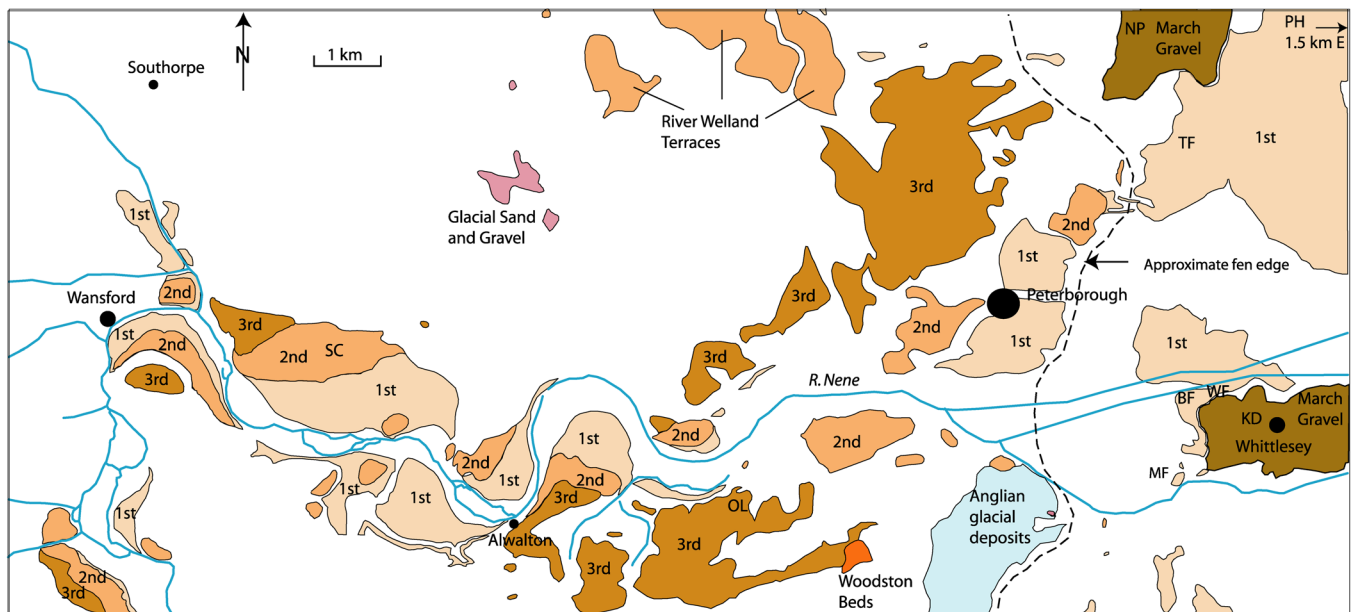
1st, 2nd & 3rd Terraces of the River Nene; SC, Sutton Cross; OL, Orton Longueville; BF, Bradley Fen; WF, West Face; KD, King's Dyke; MF, Must Farm; NP, Northam Pit; TF, Tanholt Farm; PH, Pode Hole

Figure 2. The Pleistocene geology of the lower River Nene and Peterborough area. (Redrawn from BGS, 1980, 1984, 1995a, 1995b). [Color figure can be viewed at wileyonlinelibrary.com]

reliable regional stratigraphy. Such a rationale also could be applied to other equally stratigraphically complex successions with a long-term aim of building a more complete Quaternary history of southern England.

METHODS

Fieldwork

Detailed levelling, sediment logging, two- and three-dimensional mapping and field observations (sketches, photographs) of Pleistocene deposits were carried out at sections in Bradley Fen (BFQ), King's Dyke (KDQ), Must Farm (MFQ) and West Face (WFQ) quarries (Fig. 3); the last was formerly known as Funtham's Lane East (Langford et al., 2014a). Samples were collected for the determination of clast-lithology and palaeoecology, as well as AAG, luminescence and ^{14}C age-estimates (Langford, 1999; Langford et al., 2004a, 2004b, 2004c, 2007, 2014a, 2014b, 2017, in press; Briant et al., 2018).

Clast lithology

Clast-lithology samples were dry-sieved by shaking through a nest of sieves, with the minimum sieve size being 2 mm. The clast diameter used for analysis depended on sample size: 8 mm for the smallest, 13 mm for the largest. Size fractions chosen for analysis were washed and dried prior to the clasts being sorted into five categories that reflect provenance from the bedrock and superficial geology of the River Nene catchment (flint, limestone, sandstone, ironstone and other) following Langford (1999, 2018) and Langford et al. (2004a, 2004b, 2004c, 2007, 2020). The presence of rip-up clasts of underlying Jurassic Oxford Clay, Fe-cemented and Ca-cemented aggregates, decalcified clasts, nodular chalk and *Rhaxella* chert was noted. Clasts in each of the five categories were counted, and the percentage of the total sample count was calculated. Ratios of sandstone/flint and sandstone/limestone were calculated according to the actual count for each sample.

Amino-acid geochronology

Application of AAG to the WSS includes determining the ratio of alloisoleucine to isoleucine (A/I) from *Littorina* shell fragments (Table 2, sample A2) and the amount of intercrystalline protein decomposition (IcPD) in shells of *Valvata piscinalis* and *Bithynia tentaculata* (Table 2; samples A1a and A4), as well as in *B. tentaculata* opercula (Table 2; samples A5–A9) and *Littorina* shell fragments (Table 2, sample A3). For this study, four *B. tentaculata* opercula were supplied (sample A1b, Table 2) and analysed in the same manner as previously described (Langford et al., 2007, 2014a, 2014b, 2017, in press).

Luminescence dating

Luminescence dating methods and results for samples L3 and L4 (Table 2) are presented in Langford et al. (in press), for L5–L9 in Langford et al. (2007) and for L10 and L11 in Briant et al. (2018). For the present study, quartz from samples L1, L2, L12 and L13 (Table 2) and feldspar from samples L1 and L2 were analysed at the Sheffield Luminescence Laboratory.

Dose rates for luminescence dating were based on concentrations of naturally occurring K, Th, U and rubidium (Rb) as determined by inductively coupled plasma with mass spectrometry/optical emission spectroscopy (ICP-MS/ICP-OES) at the SGS Laboratories, Ontario, Canada. An internal potassium content of 12% was assumed for feldspars, as per Lamothe et al. (1994). Elemental concentrations were converted to dose rates using data from Guérin et al. (2011). Calculations took into account attenuation factors relating to the sediment grain sizes used and the grain density. Attenuation of dose by palaeomoisture used an assumed moisture value of 20% based on present-day moisture values with a ± 5% error to incorporate fluctuations through time. Given the natural variability of sediment in close proximity to that which was sampled, dose rates were also calculated for adjacent sedimentary units, and this was factored into the gamma dose rate using data found in Aitken (1985). The contribution to dose rates from cosmic sources was calculated using

Table 1. Comparison of various stratigraphical interpretations of local Quaternary deposits.

Horton 1989[†] Holocene stage / subdivision	Horton MIS	Maddy 1999 Formation/Member	Maddy 1999 Stage	Bridgland et al., 1991 Terrestrial sequence	Bridgland Stage	Bridgland MIS	Boreham et al., 2010 Terrestrial sequence	Boreham Stage	Boreham MIS	Lee et al. (2015) Formation/Member	Lee MIS
Alluvium		Fenland Formation								Fenland Formation	1
Nordelph Peat		Must Farm Channel G / Nordelph Peat (Nene Member)								Guyhirn Member	
Barroway Drove Beds		Channel F / Barroway Drove Beds								Peat / Whittlesey Member	
Lower Peat		Lower Peat / Basal silt and soil								Peat	
1st terrace Overlying gravel	3–2	Nene Valley Formation / Ecton Member	Devensian	Upper 1st terrace	Devensian	2–4	1st terrace	Devensian	2–4	Ecton Member	5–2
Channel D	3			1st terrace	Devensian / Ipswichian	5d, 5e				Abbey Member	5e
Underlying gravel	4–3										
Channel A	5b–a			1st terrace	Late Saalian	6	1st terrace	Saalian	6	Grendon Member	6
Channel C	5e						March Gravel Sutton Cross	Saalian	7? / 7	March Gravel Member	7
Underlying gravel	6										
Channel B	7						Whittlesey 1st Terrace‖		7		
Underlying gravel	≥8										
2nd terrace		Grendon Member	Ipswichian	2nd terrace	Intra-Saalian	8?	2nd terrace	Saalian	8?	Grendon Member	8
March Gravel – PGt	5d–2	March Formation	Ipswichian	March Gravel	Intra-Saalian	9?	March Gravel	Saalian	9?	March Gravel Member	9
Sh–Sr and Fl	5e										
PGd	6										
Sd/Fd	6			Basal 2nd terrace	Intra-Saalian	10?	Basal 2nd terrace	Saalian	10?	Orton Longueville Member	10
PGcs	7										
Sm–Sr/Fm–Fl	≥8?										
3rd terrace		Orton Longueville Member	Hoxnian and later	Upper 3rd terrace	Intra-Saalian	10?	Upper 3rd terrace	Saalian	10?		
Woodston Beds		Woodston Beds	Hoxnian	Woodston Beds	Hoxnian	11	Woodston Beds	Hoxnian	11	Woodston Member	11
				Basal 3rd terrace	Anglian	12	Basal 3rd terrace	Hoxnian	11	Orton Longueville Member	12–11
Till and glacial lake		Lowestoft Formation	Anglian	Lowestoft Till	Anglian	12				Anglian Bozeat/Oadby Till	12

Abbreviation: MIS, marine isotope stage.

[†]Adapted to include the Whittlesey sedimentary succession of this study. The Must Farm succession is simplified, see text.

Table 2. Age-estimate samples from relevant sections investigated in the Whittlesey sedimentary succession, showing both those analysed for this study and those reported previously.

Section (Fig. 3)	This study sample reference	Laboratory reference	Other study sample reference	Laboratory reference	Reference
MF2	L13	Shfd21127	R6–R11		Smith et al. (2012)
	L12	Shfd21126			
MF1			R4, R5		Smith et al. (2012)
BF2			R1–R3	OxA-X-2627-56	Briant et al. (2018)
				OxA-X-2629-39	
				OxA-31962	
BF2			L10	X4210	Briant et al. (2018)
			L11	X4211	
WF3			L8	Shfd03017	Langford et al. (2007)
			L9	Shfd03021	
WF3			L5	Shfd03020	Langford et al. (2007)
			L6	Shfd03019	
			L7	Shfd03018	
KD4			L4	Shfd96130	Langford et al. (2004a)
BF3			A9	NEaar9516b–9518b	Langford et al. (2017) and Briant et al. (2018)
KD2			L3	Shfd96131	Langford et al. (2004a)
KD2			A8	NEaar13438b	Langford et al. (in press)
				NEaar 13439b	
WF3			A7	NEaar13440b–13444b	Langford et al. (in press)
WF4			A6	NEaar2655b	Langford et al. (2014a)
				NEaar2656b	
BF5			A5	NEaar4835b–4839b	Langford et al. (2014a)
WF4			A4	NEaarFLBtob	Langford et al. (2007) and Penkman (2005)
				NEaar1300b–1306b	
				NEaar1353b–1360b	
				NEaar2048b–2053b	
				NEaar2197b–2200b	
KD4			A3	NEaar5790–5792	Demarchi (2009)
KD2			A2	AAL 8518	Langford et al. (2004a)
WF3	A1b	NEaar10939b	A1a	NEaar2381b	Langford et al. (2007)
		NEaar10940b		NEaar2382b	
WF3	L2	Shfd17083			
WF5	L1	Shfd17084			

Note: Quarries: BF, Bradley Fen; KD, King's Dyke; MF, Must Farm; WF, West Face. Sample prefixes: A, AAG; L, luminescence; R, radiocarbon. AAL, Institute of Arctic and Alpine Research at the University of Colorado (Boulder).

the expression published in Prescott and Hutton (1994). Samples were prepared as per Bateman and Catt (1996) with material for dating taken from within a size range of 125–250 µm. For the small aliquot measurements undertaken, grains were mounted as a ~5 mm diameter monolayer on a 9.6 mm diameter stainless steel using silkospray. All measurements used a Risø DA-20 luminescence reader with radiation doses administered using a calibrated ^{90}Sr beta source. For quartz optically stimulated luminescence (OSL) measurements, an array of blue/green LEDs provided the stimulation while aliquots were held at 125°C and luminescence detection was through a Hoya U-340 filter. For feldspar infra-red stimulated luminescence (IRSL) measurements, stimulation was with infra-red LEDs while aliquots were held at both 50°C and 225°C and luminescence detection was through a BG3 and BG39 filter combination.

All samples were measured using the single aliquot regenerative (SAR) approach described by Murray and Wintle (2000, 2003; Supporting Information: Fig. S1; from hereon 'Supporting information' will be dropped). Five regeneration points were used to characterise growth curves, with the first regeneration point being identical to the last in order to check if sensitivity changes caused by repeated measurement of the same grains are correctly monitored and corrected for by the

SAR protocol. All aliquots where the ratio of first and last dose point exceeded ±10% of unity were excluded from further analysis.

For quartz OSL, the most appropriate preheat temperature for use within the SAR protocol was selected using a dose recovery preheat plateau test conducted on sample Shfd17083 (Fig. S2), which resulted in the selection of a preheat temperature of 200°C for 10 s. Measurement of feldspar grains used a post-IR IR protocol with the latter measured at 225°C (pIRIR$_{225}$). This protocol is thought to avoid issues related to anomalous fading but also with sufficient bleachability to potentially get reset in fluvial environments (Rhodes, 2015). The advantage of this approach over that of quartz OSL is that the IR$_{225°C}$ signal saturates more slowly, so it is able to date older samples and avoid underestimation as reported in older quartz OSL ages. The pIRIR$_{225}$ protocol used initially measured the IRSL signal at 50°C before then measuring the IRSL signal a second time at 225°C (Rhodes, 2015). The IRSL measurements were undertaken following a preheat of 225°C for 60 s as per Rhodes (2015). For both quartz and feldspar multiple aliquots of each sample were measured to better understand sample palaeodose (D_e) variability from post-depositional disturbance or partial bleaching (Fig. S3; Bateman et al., 2003, 2007; Olley et al., 2004) and SAR
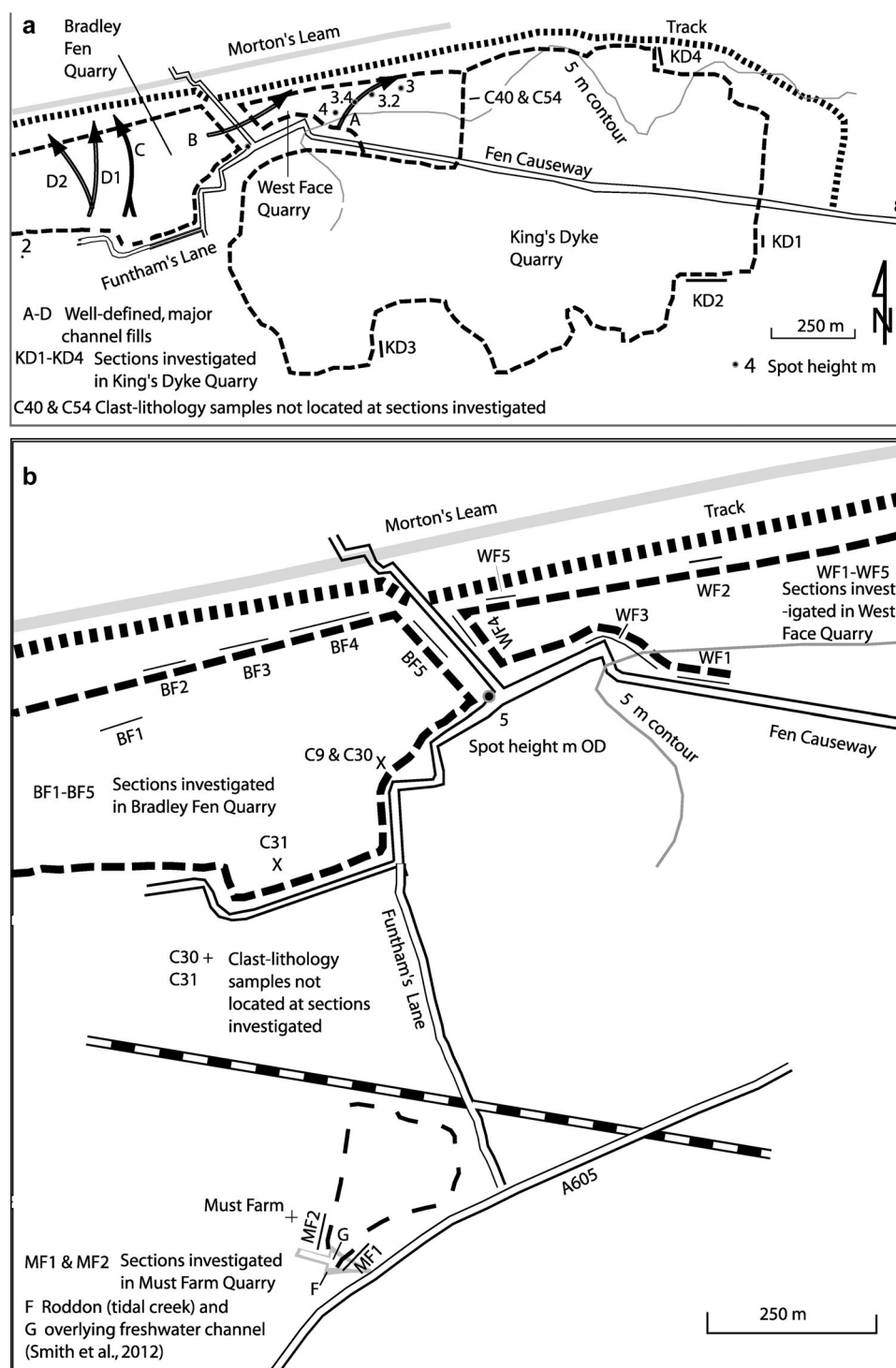
Figure 3. (a) Location of the King's Dyke, West Face (formerly Funtham's Lane East) and Bradley Fen quarries in Whittlesey, where exposures of Quaternary deposits have been studied and individual sections investigated. Location of major channels A–D are also shown. (b) Location of Must Farm Quarry and channels F and G, relative to Bradley Fen and West Face quarries.

growth curves for signs of saturation and aliquots at or beyond the limit of the measurement method used (Murray and Funder, 2003).

Radiocarbon dating

Radiocarbon dating of *Carex* and *Potamogeton* seeds (samples R2 and R3, Table 2) from Late Pleistocene deposits utilised a strong acid–base–acid pretreatment protocol detailed in Briant et al. (2018). In addition, a foot bone from a woolly rhinoceros (*Coelodonta antiquitatis*) found *in situ* within the channel deposits

immediately adjacent to the location of the sample containing *Carex* and *Potamogeton* seeds was radiocarbon dated using an ultrafiltration pretreatment (sample R1, Table 2). For the Holocene part of the sequence (samples R4–R11, Table 2), the radiocarbon dates are taken from Smith et al. (2012). Thus the Holocene sediments at the specific sections reported here have not been radiocarbon dated directly, rather their age is estimated from a time-stratigraphic framework based on radiocarbon dates reported from surrounding peats up to 2.5 km away (R4, R5 and R8–R11), augmented by radiocarbon dates for a foraminifera and freshwater mussel from channels F and G respectively in Must Farm Quarry

(R6 and R7). In addition, radiocarbon dates on archaeological material document the corresponding rise of water level (0, ~0.25, 0.5, 1 and 1.5 m OD) in Bradley Fen Quarry (from Knight and Brudenwell, 2020).

Stratigraphical interpretation

Stratigraphical interpretation of the Pleistocene deposits was based on sedimentology, observed field relationships, clast lithology, palaeoecological data, age estimates and biostratigraphy. Sedimentary characteristics were used to establish two- and three-dimensional facies architecture and, combined with ecological data, to interpret depositional environment, leading to the determination of sedimentary facies associations (Reading, 1996; Jones et al., 1999). Standard methods were used for palaeoecological interpretation, as detailed in Langford et al. (2007, 2014a, 2014b, 2017), where the rationale for the relevant Pleistocene biostratigraphy can be found. Additional information is included below as appropriate. Information on the Holocene sequence is drawn from Smith et al. (2012), Knight and Brudenwell (2020) and Knight et al. (2024).

RESULTS

Sedimentology, site-stratigraphy, palaeoecology, clast-lithology and age-estimate results from this and previous studies were integrated in order to determine the sedimentary facies association and plausible stratigraphical interpretation (i.e. grouping within and order of the facies associations). Twenty sedimentary facies associations (W1–W20) were identified accordingly (Table 3); W8(WF) and W8(KD), W9(WF) and W9(KD) and W10(BF) and W10(KD) each represent potentially coeval separate facies associations in the respective quarries; in addition, W15(KD) is recognised as coeval with W15 in WFQ and BFQ. Detailed description of sedimentary characteristics for the relevant facies associations is provided in Table 3. Fig. 4 provides a schematic summary of the disposition of facies associations W1–W3, W5–W8, W10–W12, W14 and W15 in West Face and Bradley Fen quarries in order to clarify some of the stratigraphical complexities that have emerged. (Figs. S4–S6 show the two-dimensional architecture of Pleistocene facies associations W1–W18, their spatial distribution, as far as is known, and interpreted aggradational history). Determination of Holocene facies associations W19 and W20 that crop out in Must Farm Quarry (MF; Figs. 3(b) and 5(a)) was based on information in Smith et al. (2012) and one-dimensional sedimentary logging at section MF2 (Fig. 5(b)). From hereon, for the sake of brevity, MIS climatic stages and substages will be used in preference to national and regional stratigraphic terms where appropriate because they are recognised internationally. In doing so, qualifying phrases such as 'equivalent to' or 'climatic (sub) stage' are intended but may not be used.

Facies association W1

Its high flint content (>50%; Fig. 6 and Table S1) distinguishes W1 from all other facies associations except W15. Demonstrably underlying W2, and therefore robustly dated channel B (W5 and W6, Fig. 4), it has an upper bracketing age of MIS 7. Flint present in W1 provides a lower bracketing age of MIS 12, when Cretaceous material from the northeast was first introduced into the area during the Anglian glaciation (Horton, 1989; Langford, 2004, 2011). As the fossil assemblages of the

boulder-size rip-up clasts of stratified organic mud (OMC, Fig. 4) indicate cool/cold climatic conditions, W1 has a notional minimum age of MIS 8. Unfortunately, attempts by OSL and pIRSL$_{225}$ dating to determine which cold stage, MIS 10 or 8, proved inconclusive. For sample L1 (Table 4), 112 ± 8 ka was measured on quartz and 162 ± 10 ka measured on feldspar. These are not within error of each other, and both are post MIS 7 in age, contrary to the AAG of the overlying channel B. This age underestimation is not due to saturation of the quartz OSL signal or overestimation of the dose rate owing to too low a palaeomoisture estimate being used, and the dose rate for this sample is in line with others in this study. The cause of the age underestimation remains to be investigated, but for the purposes of this paper, these ages were not considered further.

Facies association W2

An increase in limestone and sandstone at the expense of flint (Fig. 6 and Table S1) in the clast-lithology assemblage characterises W2 compared with W1. The top of W2 in section WF3 (FH, Fig. 4) forms part of a post-W6 (but pre-W8) induration event, hence the presence of Fe-cemented aggregates in clast-lithology sample C7. Palaeoecological data are limited to unpublished mollusc and ostracod assemblages from a sand lens at the junction of sections BF4 and BF5 (Fig. 3(b); Tables S2 and S3(a)). *Valvata piscinalis* dominates the molluscan fauna and *Prionocypris zenkeri* the ostracod fauna. The assemblages are not diagnostic biostratigraphically, nor do they indicate accumulation under cold conditions. The presence of ostracods *Cytheromorpha fuscata* and *Heterocypris salina* hints at brackish water, perhaps indicating a tidal connection or at least proximity to the sea, and thus temperate conditions and high relative sea level (RSL), but an alternative explanation that these assemblages contain locally re-worked elements from earlier temperate deposits cannot be ruled out. As W2 underlies channel B (Fig. 4), it has an upper bracketing age of MIS 7, and underlying W1 provides a notional minimum lower bracketing age of MIS 8. The presence of boulder-size rip-up clasts of stratified organic mud (OMC, Fig. 4) suggests correspondence in age with W1. Ages of 179 ± 13 ka measured on quartz and 168 ± 10 ka measured on feldspar (sample L2, Table 4) were obtained for W2. These are within error of each other but are inconsistent with the pre-MIS 7 AAG age of overlying channel B. Although having high D_e values, neither the OSL nor the pIRSL$_{225}$ samples were saturated. The cause of the age underestimation remains to be investigated, but for the purposes of this paper, these ages were not considered further.

Facies association W3

High limestone and sandstone content characterises W3 (Fig. 6 and Table S1), something not evident in the assemblage of sample C30 (Figs. 3(b) and S5(c) (ii); Table S1), thus constraining the southern limit of W3 in BFQ. Later incisions (W8 and W10 in WFQ and BFQ, respectively) have obscured the age relationship between W2 and W3 (Fig. 4), and only in the temporary section I1 in BFQ (Fig. S7; Langford et al., 2004c) was it apparent that W3 truncated W2 and hence is younger. As W3 in BFQ was incised by channel B (Fig. 3(a)), it has an upper bracketing age of MIS 7, and the incision of W2 indicates a notional minimum lower bracketing age of MIS 8. An indurated horizon caps W3 at section BF4 in BFQ, formed by secondary Ca-cementation (CH, Fig. 4; Table S1, C10 and

Table 3. Facies associations, architectural elements (Church, 1974), description and interpreted depositional environment of facies associations W1–W20.

| Facies association[a]	Element (major; minor lithofacies)[b]	Brief description	Interpretation
W20: MF	Channel fill, overbank heterolithic sheet, peat (Fm, Fl, Sh, Sm)	Structureless silty clay to clayey silt with pockets and lenses of stratified or structureless silts to sands incised by laminated silt and sand channel fill and structureless muddy channel fill, overlain by peat	Upward cycle of water level rise and landscape drowning as a result of a combination of sea-level rise and glacio-isostatic adjustment (GIA), interspersed with tidal creek and fluvial drainage development
W19: MF	Heterolithic and silt sheets, peat (Sm, Fm)	Soil development overlain by structureless silt, in turn overlain by peat	Upward cycle of water level rise and landscape drowning as a result of a combination of sea-level rise and GIA
W18: BF, MF	Gravel sheet (PGmc–PG(s)c; Sh–Sm, Fl–Fm)	Clast-supported structureless laterally extensive gravel sheets with isolated cut-and-fill horizontally stratified to structureless lenses of silt to coarse sand	Accumulation of gravel sheets during nival flood events and bar-top reworking during less energetic events.
W17: BF	Sandy channel fill (Sh, St, Sp, Sm; Fl, Fm)	Lateral and vertical aggradation of stratified sands and minor fines	Shallow sand-bed braided stream
	Heterolithic channel fill (Fm; PGmc)	Structureless organic mud channel fill	Episodic infilling of a single-thread muddy channel. Palaeoecology indicates deposition under cold conditions
W16: BF	Gravel sheet (PGmc–PG(s)c; Sh–Sm, Fl–Fm)	Clast-supported, structureless, laterally extensive gravel sheets with isolated cut-and-fill horizontally stratified to structureless lenses of silt to coarse sand	Accumulation of gravel sheets during nival flood events and bar-top reworking during less energetic events. Development of ice-wedge casts indicates deposition under cold conditions
W15: WF, BF	Gravel sheet (PGmc–PG(s)c; Sh–Sm, Fl–Fm)	Clast-supported, structureless gravel sheet with isolated cut-and-fill horizontally stratified to structureless lenses of silt to coarse sand. Locally, lenses of reworked decalcified sand and gravel are present	Accumulation of gravel sheets during nival flood events and bar-top reworking during less energetic events. Cryogenic deformation indicates deposition under cold conditions
W15: KD	Gravel sheet (PGmc, PGt–St; Sh–Sm)	Lateral and vertical aggradation of cut-and-fill trough cross-bedded gravel and sand. Evidence for small-scale syngenetic cryogenic deformation. Locally, lenses of reworked decalcified sand and gravel are present	Aggradation by migrating streams in a permafrost environment under an arctic nival discharge regime. Syn- and post-depositional cryogenic deformation indicates deposition under cold conditions
W14: BF, WF	Gravel channel fill and heterolithic sheet (PGmc–PG(s)c, Fm; St–Sh–Sm)	Channelised clast-supported, structureless gravels that upwards are interbedded with laterally persistent cut-and-fill horizontally stratified lenses of silt to coarse sand, passing laterally into structureless silt-dominated heterolithic deposits to the west	Single-thread gravel-bed river with heterolithic overbank deposits
W13: KD	Sand–silt channel fill (Sh–Sm, Fl)	Medium horizontally stratified to structureless sand overlain by wavy laminated fine sand to silt containing foraminifera and ostracods	Distal inner estuarine/marine-connected fluvial. Palaeontology indicates deposition under temperate conditions
W12: BF	Heterolithic channel fill/ point bar and transition to overbank fines (PGmc; S–Fm; PGsc; S–Fm)	Interbedded pebbly, clast-supported gravel and fossiliferous silts with low-angle stratification overlying pebbly, clast-to-matrix-supported, structureless muddy gravel with pockets of organic-rich silt to fine sand	Sinuous single-thread channel with point-bar development. Palaeoecology indicates deposition under temperate conditions
W11: BF	Heterolithic channel fill (Fm; PGm, Sm)	Shell-rich sand and gravel pockets in a structureless heterolithic matrix	Cohesive flow deposits
W10: BF	Gravel sheet (PGpc, PGtc)	Clast-supported, structureless gravels and large-scale cross-bedded sand and gravel indicate southward flow. Post-depositional cryogenic deformation is evident	Large-scale gravel-bed braided river. Post-depositional cryogenic deformation indicates deposition under cold conditions
W10: KD	Cryogenically deformed gravel (PGd)	Large-scale involutions of pebbly, clast-supported structureless gravel within the underlying sands and muds of W9	Original depositional environment could not be determined because of the intensity of cryogenic deformation
W9: KD	Sand sheet and muddy channel infill (Sh, Sd, Fd; PGmc, PDmm)	Horizontally stratified sands, with minor laminae of silt–clay and, locally, transition from low-angle cross-stratification to type B ripple-drift cross-stratified sand separated from structureless organic mud with minor ribbons of silt and pockets of pebbly, clast-supported, structureless gravel by a singular pocket of pebbly, structureless diamicton. Extensive evidence of post-depositional cryogenic deformation	Sand-bed stream deposits and abandoned channel infill on a high-level terrace of a braided stream. Pollen from the structureless muds indicates deposition under cool conditions
W9: WF	Gravel sheet and muddy	Pebbly, clast-supported, structureless gravel	Cyclic? deep incision with episodic infilling.

(Continued)

Table 3. (*Continued*)

Facies association[a]	Element (major; minor lithofacies)[b]	Brief description	Interpretation
	channel fills (PGmc, Fm–Fl)	with a sequence of vertically stacked, organic, structureless to stratified mud channels	Palaeontology indicates deposition under cold conditions
W8: KD	Inclined pebbly gravel beds and heterolithic channel fill (PGcs, Fm–Fl, Sm–PGm)	Fossiliferous, structureless to stratified clayey silts interbedded with fossiliferous coarse sand ribbons containing scattered pebbles and *Littorina* shells overlie a wedge of pebbly, stratified gravel beds, shallowly inclined to the east	Fluvial bar-top reworking and infilling of shallow depression. Palaeoecology is not diagnostic except for interglacial foraminifera confined to one of the sandy ribbons
W8: WF	Gravel channel fill (PGcm, PGt–St; Sm, Fm–Fl)	Pebbly, structureless, clast-supported beds of gravel, with continuous ribbons of fossiliferous, sandy silt/clay at the base of each bed, underlying a thin, laterally persistent, fossiliferous, sand ribbon (maximum thickness 5 cm) that separates the lower gravel from fossiliferous, pebbly, trough cross-stratified, clast-supported gravel and trough cross-stratified sand	Near-coastal, ephemeral gravel-bed stream with permanent stream conditions developing at the top. Palaeoecology indicates deposition under temperate conditions
W7: BF, WF	Sand–silt sheet (St–Fl; Fm)	Shallow, intercalated trough cross-stratified sand to silt channel fills	High water-table floodplain. Palaeoecology indicates deposition under temperate conditions and a falling water table at the top
W6: BF, WF	Gravel–sand channels in a silt-dominated heterolithic sheet (PGt–St, Fm–Fl, Sm–St)	Fossiliferous, pebbly, clast-supported trough cross-stratified gravel and sand lenses and pockets interbedded with structureless to stratified clayey to sandy silt	Active single-thread channel and proximal floodplain. Palaeoecology indicates deposition under temperate conditions
W5: WF	Heterolithic channel fill/ point bar/overbank heterolithic sheet (PGmc/Sm–Fm, PG(s)incc, Sm–Fm)	Fossiliferous, muddy and coeval weakly low-angle stratified, pebbly, clast-supported gravel; shell-rich dark organic mud; olive grey sandy to clayey silt with common pockets of medium to coarse sand containing comminuted shells	Abandoned channel of sinuous single-thread stream and heterolithic overbank deposits. Palaeoecology indicates deposition under temperate conditions
W4: KD	Gravel sheet (PGm–(s)c; St/Sp)	Pebbly, clast-supported, structureless to weakly stratified gravels with minor stratified sand and gravel infilling shallow channels and troughs	Planar gravel sheets or longitudinal bar forms under high-energy flood conditions
W3: BF	Gravel sheet (PGmc)	Poorly exposed, pebbly, clast-supported structureless gravel with an indurated horizon at the top formed by secondary Ca	Insufficient data
W3: WF	Gravel sheet (PGmc/PG(s)incc; Fm–Fl)	Pebbly, clast-supported structureless to weakly stratified gravel marked by low-angle discontinuity surfaces, suggesting aggradation from west to east. There are two laterally continuous beds of organic mud separated by a thin bed of gravel at the top	Bar top adjacent to a stream bank. Palaeoecology indicates a moderately cold temperature
W2: BF, WF	Gravel sheet (PGs(hor)c, PGshorc/PGp, PGt; Sp, Sshor, Fm)	Pebbly, horizontally to subhorizontally stratified, clast-supported gravel sheets predominate, with subordinate shallow channel fills of pebbly, planar cross-bedded gravel and sand and pebbly, trough cross-bedded gravel and sand	Accumulation of gravel sheets during nival flood events and bar-top reworking during less energetic events
W1: WF	Diamictic–gravel channel fill (PDmm, PDsincm-c, PGsincm-c; Sshor)	Pebbly, structureless, matrix-supported diamicton passing downslope into low-angle stratified matrix-supported diamictons and further downslope into pebbly, low-angle stratified, clast-supported gravel, with rare horizontally stratified sand lenses and several boulder-sized rip-up clasts of organic stratified muds	Subaerial sediment erosion, mobilisation and downslope deposition in a low-energy body of water. Palaeoecology indicates a cold climate

Abbreviations: Fl, stratified fines; Fm, massive (structureless) fines; PDmm, massive, matrix-supported pebbly diamicton; PDs$_{inc}$m-c, stratified (inclined) matrix- to clast-supported pebbly diamicton; PGm–(s)c, clast-supported, massive to weakly subhorizontally stratified pebbly gravel; PGp, pebbly, planar cross-stratified gravel; PGs$_{hor}$c, clast-supported, horizontally stratified pebbly gravel; PGs$_{(hor)}$c, clast-supported, subhorizontally stratified pebbly gravel; PGs$_{inc}$m-c, matrix- to clast-supported, stratified (inclined) pebbly gravel; PGt, pebbly, trough cross-stratified sand; Sm, massive sand; Sp, planar cross-stratified sand; Ss$_{hor}$, horizontally stratified sand; St, trough cross-stratified sand.
[a]Quarry location indicated: BF, Bradley Fen; KD, King's Dyke; MF, Must Farm; WF, West Face.
[b]Lithofacies codes adapted from Miall (1977) and Dardis (1984). The gravel clast-size prefixes denote the largest size commonly present, that is, not the average clast size.
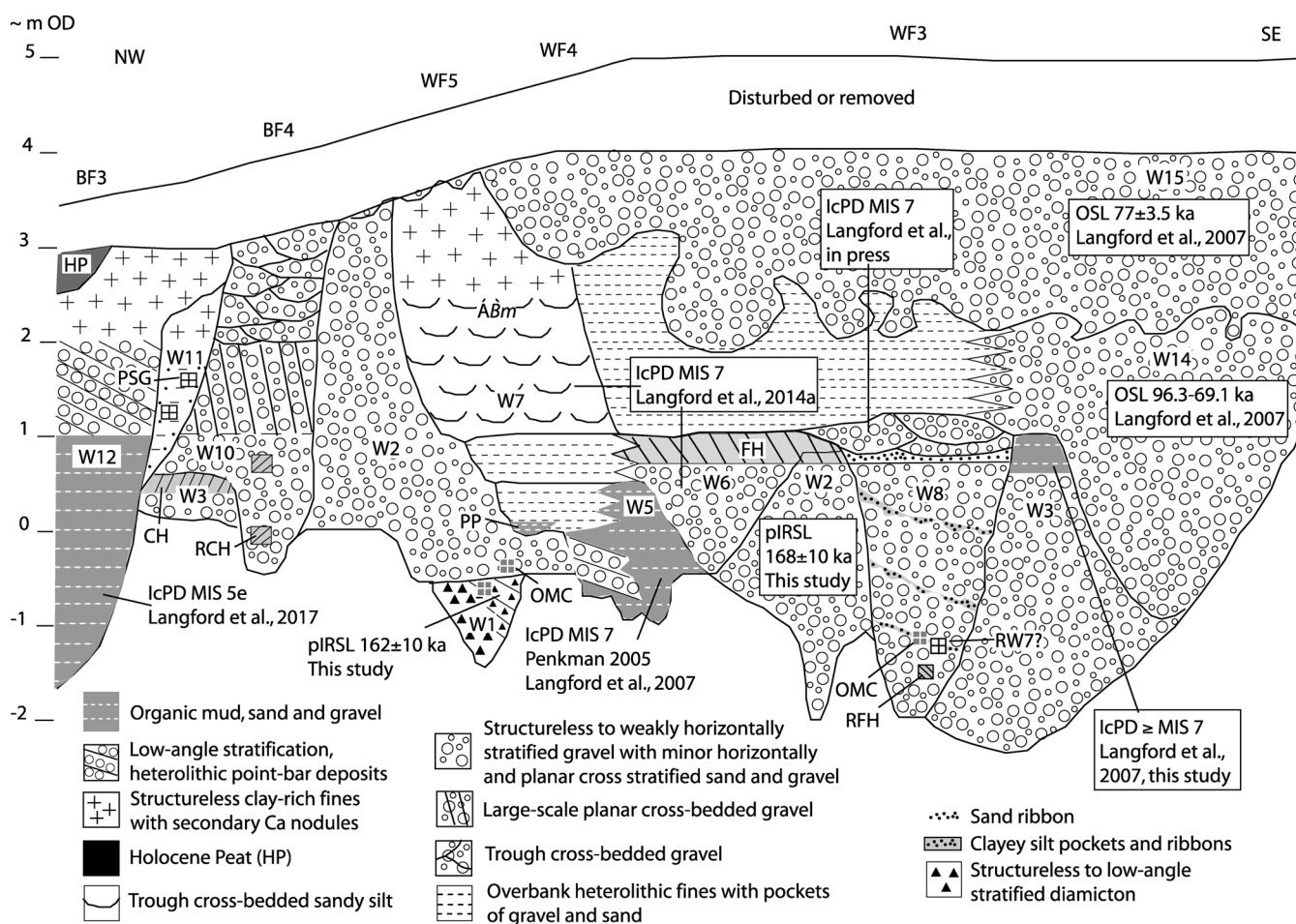
Figure 4. Simplified cross-section showing stratigraphical relationships for facies associations W1–W3, W5–W8, W10–W12, W14 and W15 in WFQ and BFQ.

C11; Langford et al., 2004c, where it is incorrectly referred to as Fe-cemented). Although Ca-cemented aggregates in W10(BF) provide an upper bracketing age of MIS 6 for the secondary Ca-cementation, it is likely to have been formed under the high water table conditions necessary for aggradation of W7 (see later), which is dated to MIS 7 by opercula AAG (Table 2, sample A6), thus supporting W3's notional minimum MIS 8 age in BFQ.

Organic mud beds (Fig. 4) cap the heavily Fe-stained W3 in WFQ (Table S1, C12). Subsequent incision by MIS 7 aged W8 (A7, Table 2) provides an upper bracketing age. Earlier AAG dating of W3 at WF3 (Langford et al., 2007) utilised IcPD analyses on *B. tentaculata* and *V. piscinalis* shells and *B. tentaculata* opercula from the organic mud beds, with the latter represented by sample A1a (Table 2). Results for A1a indicated an older age for the W3 specimens than those from W5 (A4, Table 2), but caution was advised considering the small sample number so four more *B. tentaculata* opercula (A1b, Table 2) were analysed for this study and results (for both A1a and A1b) are shown (by W3 plots) in Fig. 7(a), (b), with the relevant data listed in Table S4. Although an MIS 7 age is depicted in Fig. 7(a), a greater degree of decomposition is shown in bivariate plots of 'free' versus hydrolysed data for Asx, Glx, Ala and [Ser]/[Ala] of W3 opercula than for all other opercula from this site analysed by this method (Fig. S8(a)). Together, these

data suggest an age earlier in MIS 7 than W5–W8(WF), or an age older than MIS 7. The fossil assemblage of the organic mud beds indicates accumulation under cold/cool conditions, implying accumulation or bar-top reworking of W3 in a cold MIS 7 substage (the implication of this possibility for MIS 7 climatic substage stratigraphy is explored in the Appendix) or in a pre-MIS 7 cold stage. The presence of the temperate molluscan species *Azeca goodalli* indicates some reworking of earlier interglacial deposits, and if the dated material was also reworked, the level of IcPD suggests reworking of MIS 7 or 9 rather than MIS 11 fauna. Hence, deposition of W3 would be no older than MIS 8.

Facies association W4

Its high limestone content distinguishes W4 from W1–W3 (Fig. 6 and Table S1). The stratigraphical relationship between W1–W3 and W4 cannot be established with certainty on the evidence available. The clast-lithology data suggest that W4 is younger based on the small increased flux of sandstone (sample C14, Table S1) downstream of W3 in WFQ (Fig. S5(a) (iv)), which is rich in sandstone. Palaeoecological data are limited to unpublished microfauna data from a sand lens in section KD3 and a mud clast in section KD4 (Fig. 3; Table S3b). Of note is
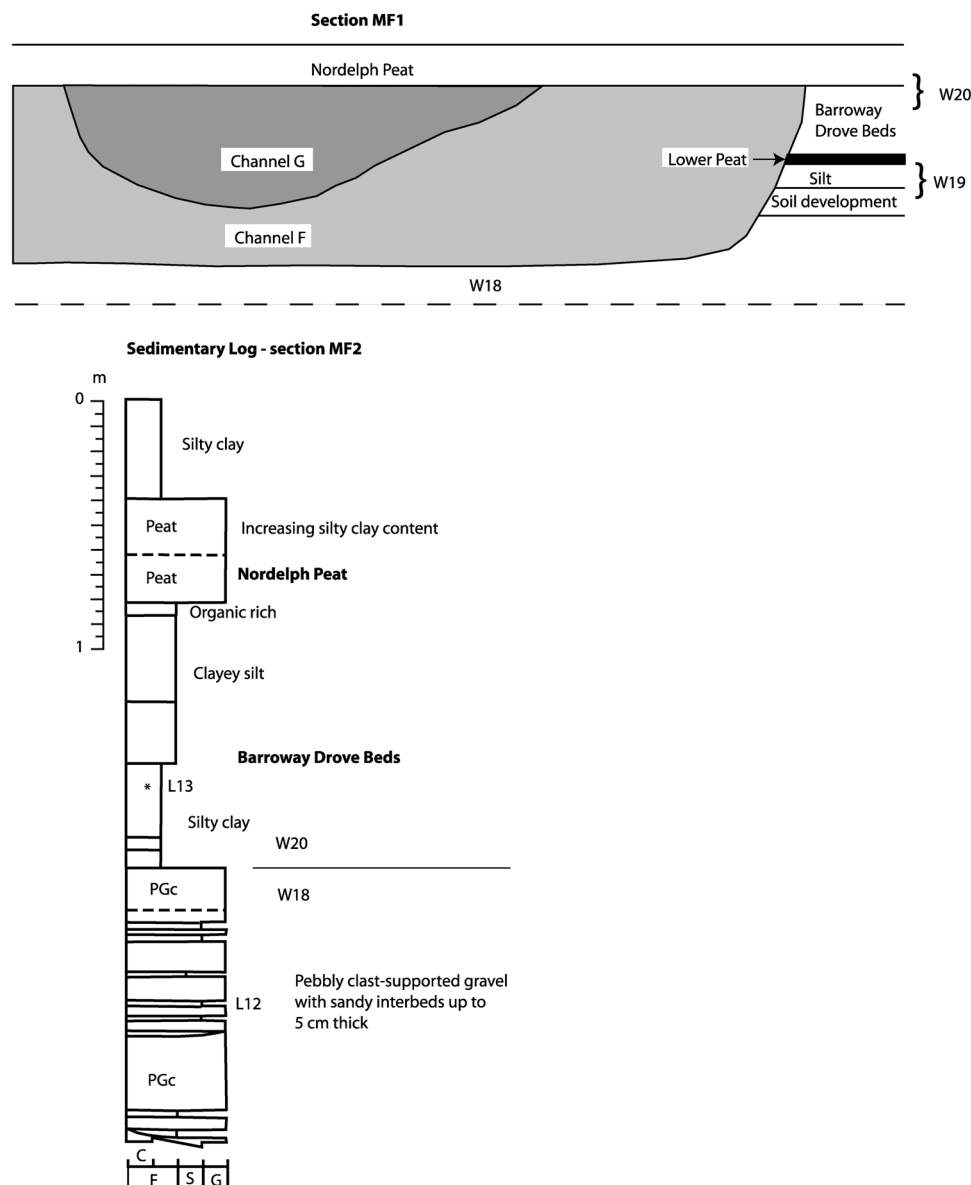
Figure 5. Schematic cross-section of facies associations W19 and W20 at section MF1 (after Smith et al., 2012) and sedimentary log at section MF2 in Must Farm Quarry, Whittlesey.

the abundance in both samples of the ostracod *P. zenkeri* (as in the sample from W2), characteristic of streams and springs, and the presence of the cool/cold indicator ostracod *Leucocythere batesi*, also found in the fauna of W1. A few foraminifera are present, as well as a few outer estuarine/marine ostracods, but these are likely to have been reworked. An upper bracketing age of MIS 7 is provided by opercula AAG dating of overlying W8(KD) at section KD2 (Table 2, sample A8; Fig. 7(b)). A maximum age of MIS 8 is suggested if, as outlined above, the increased flux of sandstone at section KD4 is derived from W3 at WFQ. A maximum age of MIS 8 is also supported by the increased level of IcPD in *Littorina* shell fragments found adjacent to the fossiliferous mud clast in section KD4 (Table 2, sample A3; Demarchi, 2009) when compared with the MIS 7 mean and standard deviation data for multiple amino acids (Asx, Glx, Ala and Val) from Easington (Davies et al., 2009) in Fig. 7(b). The distinction is obscured by an overlap of the *Littorina littoralis* data set from Easington with the W4 data set for Glx, Ala and Val, as demonstrated by bivariate plots of 'free' versus hydrolysed data (Fig. S8(b)). A clear distinction is apparent when the

hydrolysed data for Val versus Asx are compared (Fig. 7(c)), regardless of species, with the W4 material appearing to be older than that at Easington. As for W3, the level of IcPD suggests reworking of MIS 9 rather than MIS 11 material. Further support is provided by data on the ratio of A/I from *Littorina* shell fragments in W4 at section KD2 (Table 2, sample A2; Figs. 7(d) and S4). J. Hollin (personal communication, 1998) considered his unpublished *Littorina* ratios of 0.13 and 0.30 to correspond to MIS 5e and MIS 11, respectively, but recent luminescence dating indicates that the ratio 0.13 corresponds with MIS 7. The mean ratio of 0.25 for W4 he regarded as being compatible with MIS 9, though MIS 11 could not be ruled out. The fragments of *Littorina* shell in W4 are considered to be derived from previous interglacial sediments, which the A/I data suggest most likely had an age corresponding to MIS 9, thereby limiting the timing of reworking to MIS 8.

Facies association W5

This facies association comprises the fossiliferous basal muddy gravel, point-bar, abandoned muddy channel and overbank
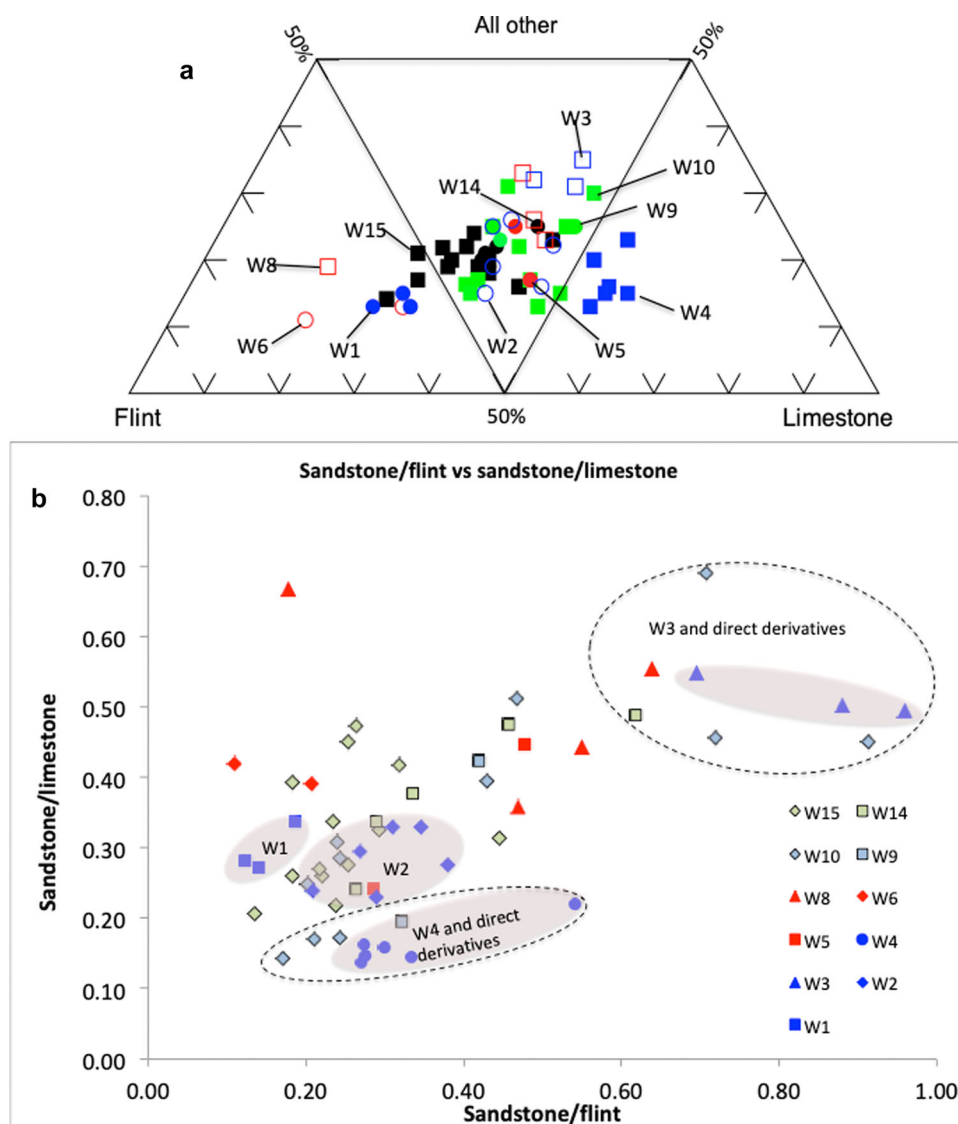
Figure 6. (a) Percentage flint versus limestone versus all other lithologies by relevant facies association. (b) Sandstone/flint versus sandstone/limestone ratios by relevant facies association. [Color figure can be viewed at wileyonlinelibrary.com]

Table 4. Published and unpublished (this study) luminescence age estimates.

FA	Sample number	Laboratory code	Dose rate (Gy kyr^{-1})	Mineral/method	Palaeodose (D_e) (Gy)	Age (ka)
W20 (TS)	L13	Shfd21127	1.476 ± 0.081	Qtz/OSL	21.6 ± 0.5	14.6 ± 0.87
W18 (TS)	L12	Shfd21126	0.767 ± 0.042	Qtz/OSL	11.3 ± 0.5	14.7 ± 1.04
W16	L11	X4210	1.00 ± 0.06	Qtz/OSL	40.4 ± 3.2	41.6 ± 4.3
	L10	X4211	0.99 ± 0.06	Qtz/OSL	44.9 ± 3.1	44.6 ± 4.2
W15	L9	Shfd03021	1.876 ± 0.077	Qtz/OSL	194 ± 6.0	103 ± 5.4
	L8	Shfd03017	1.211 ± 0.048	Qtz/OSL	94 ± 2.1	77 ± 3.5
W14	L7	Shfd03018	0.801 ± 0.076	Qtz/OSL	152 ± 5.3	89 ± 5.0
	L6	Shfd03019	1.962 ± 0.090	Qtz/OSL	142 ± 5.0	73 ± 4.2
	L5	Shfd03020	1.726 ± 0.078	Qtz/OSL	157 ± 5.7	91 ± 5.3
W13	L4	Shfd96130	1.315 ± 0.079	Qtz/OSL	151.9 ± 19.36	116 ± 16
W9(KD)	L3	Shfd96131	1.340 ± 0.083	Qtz/OSL	211.96 ± 12.99	158 ± 14
W2 (TS)	L2	Shfd17083	1.962 ± 0.115	Feld/pIRIR$_{225}$	329 ± 4.2	168 ± 10
			1.295 ± 0.074	Qtz/OSL	231.3 ± 9.5	179 ± 13
W1 (TS)	L1	Shfd17084	2.254 ± 0.132	Feld/pIRIR$_{225}$	365 ± 8.6	162 ± 10
			1.769 ± 0.082	Qtz/OSL	176.9 ± 8.2	112 ± 8

Abbreviation: FA, facies association; TS, this study. Sources: Langford et al. (2004a, 2007); Briant et al. (2018).

facies of channel B (Fig. 3(a)), which is part of a complex sequence of opercula AAG dated deposits (Table 2 (samples A4–A7) and Table S4; Figs. 7(b) and S8(a)) attributed to the penultimate interglacial (Fig. 4), comprising W5–W8(WF); of this complex only this lower part of channel B has been reported in

detail. Facies associations W6–W8(WF) are also very fossiliferous, but analyses of the Mollusca and microfauna remain incomplete. Clast lithology of the muddy gravel is similar to that of the underlying W2 (Fig. 6 and Table S1, C19 and C20). Comprehensive IcPD analyses of 25 *B. tentaculata* opercula
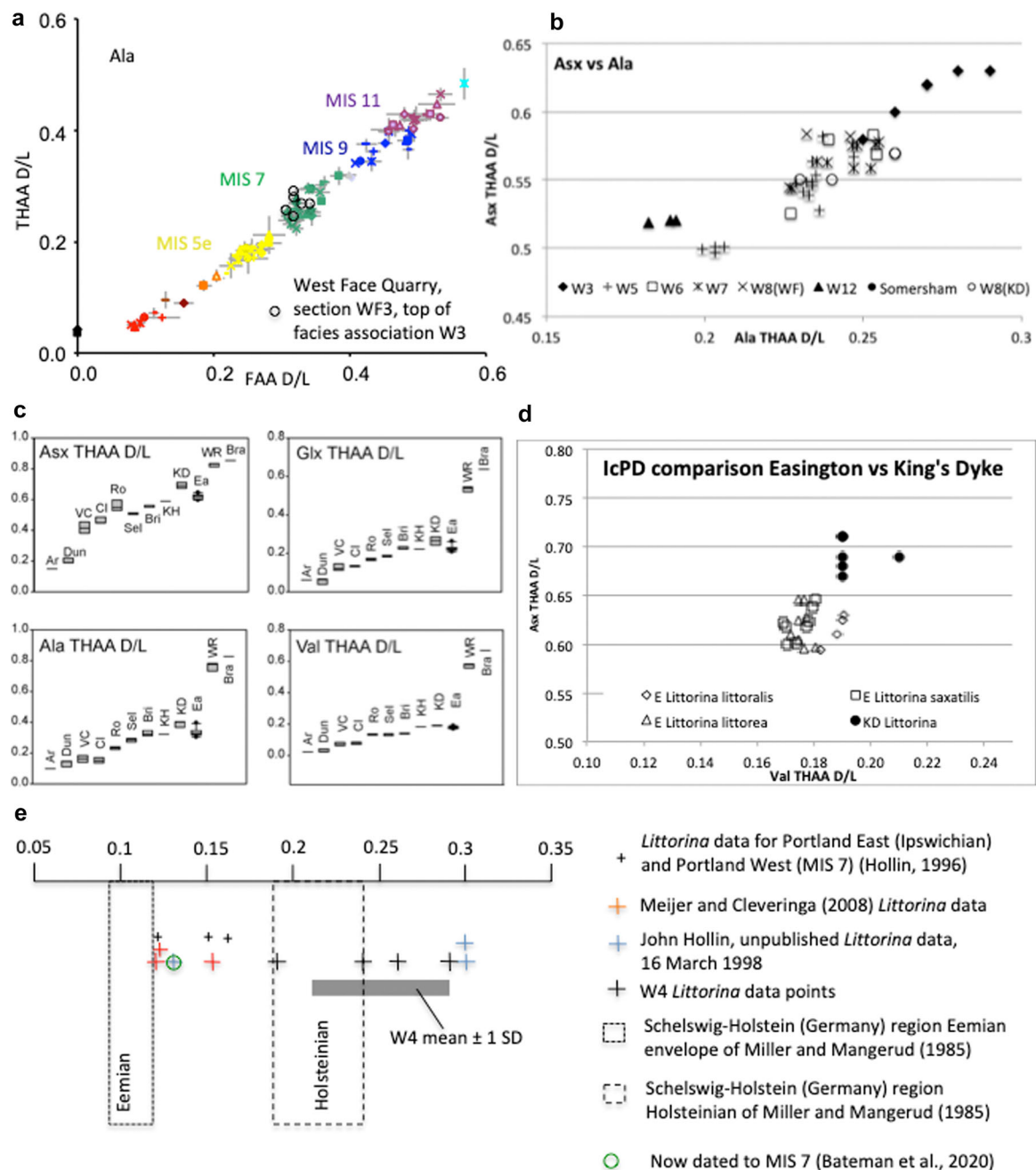
Figure 7. (a) Alanine IcPD data for *B. tenataculata* opercula from W3 (samples A1a and A1b, Table 2) in WFQ plotted against mean THAA D/L versus FAA D/L data for the British Isles. (b) Plots of hydrolysed Asx versus Ala IcPD data for *B. tenaculata* opercula from W3(KD), W5–W8 and W12 (samples A4–A9, Table 2). (c) Comparison of IcPD data for *Littorina* from W4 (KD; sample A3, Table 2) at section KD4 in KDQ with IcPD data on *Littorina* from other British sites: Ar, Archerfield; Dun, Dunbar; VC, North Sea core; Cl, Clacton; Ro, Rotherslade; Sel, Selsey; Bri, Brighton; KH, Kelsey Hill; Ea, Easington; WR, West Runton; Br, Bramerton. (Figure supplied by B. Demarchi.) (d) Comparison of hydrolysed Val versus Asx IcPD data for *Littorina* from Easington and W4 (data supplied by B. Demarchi). (e) Comparison of A/I *Littorina* AAR data for facies association W4 at section KD2 in KDQ (sample A2, Table 2) with data from Meijer and Cleveringa (2009), Hollin (1996; J. Hollin, personal communication, 1998) and Miller and Mangerud (1985). [Color figure can be viewed at wileyonlinelibrary.com]

(Penkman et al., 2011, 2013), and 25 *B. tentaculata* and 25 *V. piscinalis* shells (Penkman, 2005) provide an MIS 7 age.

Facies association W6

Forming the upper part of channel B (Fig. 4), W6 comprises gravel with common lenses of sand in the main channel and isolated or coalescing gravel and sand lenses interbedded with silt and clay overbank deposits elsewhere, representing a gravel-bed stream that flowed to the northeast. Varied sizes of *Corbicula* cf. *fluminalis*, with articulated specimens common, dominate bands and pockets of shells throughout the main

channel gravels. The fully temperate molluscan fauna of the main channel is very similar to that of the basal muddy gravel facies of W5 (Table S5; Fig. S6); dominated by *V. piscinalis*, *Belgrandia marginata*, *B. tentaculata*, *Radix* spp., *Ancylus fluviatilis*, *C.* cf. *fluminalis* and *Pisidium moitessierianum*, and includes *T. danubialis*. Likewise, the fully temperate ostracod assemblage of the main channel facies is very similar to that of the basal muddy gravel facies of W5 (Table S6), with a high proportion representing brackish upper estuarine conditions. As in W5, the only brackish indicators in W6 are the two ostracods *Cyprideis torosa* and *C. fuscata* among an otherwise freshwater assemblage, perhaps suggesting extreme tidal or

storm surge influxes upstream of the normal tidal limit, and thus sea level similar to today, although both species can live in fresh waters. Preliminary geochemical data for *C. torosa* confirm that the shells calcified in low salinity water, presumably freshwater with a small admixture of seawater (J. Holmes, personal communication, 2025). Where it overlies W2, clast-lithology samples from the top of the main channel facies indicate an indurated horizon (FH, Fig. 4), with the presence of Fe-cemented aggregates, a notable increase in flint, a decrease in limestone, near absence of ironstone and presence of decalcified limestone clasts (Fig. 6 and Table S1, C21 and C22). The opercula AAG dating of W6 provides a lower bracketing age of MIS 7 for both W7 and W8(WF) (Fig. 4).

Facies association W7

A broad sheet of intercalated lenses of silts to silty sands forms W7 at the western and eastern ends of WFQ and BFQ, respectively (Fig. 4). Langford et al. (2004b) provide a comprehensive list of molluscs (their table 10, sample 57) for the base of W7 (Fig. S9). Sedimentary characteristics and their molluscan fauna (characterised by *Valvata cristata*, *Bithynia troschelii*, *Anisus* spp., *Gyraulus* spp., *Acroloxus lacustris*, *Pisidium milium* and rarity or absence of *C.* cf. *fluminalis*, *T. danubialis* and *A. fluviatilis*) indicate slow-moving to standing water and high-water-table conditions in which *Chara* grew profusely, forming a *Chara* marl (Fig. S9). This assemblage characterises the sequence, except for the significant appearance of largely complete and well-preserved *B. marginata* at its top (Table S7, samples G6 and G7), suggesting a fall in the water table, reappearance of subaerial springs and possible change in depositional environment; this is supported by an abundance of the ostracod *Psychrodomus olivaceus*, characteristic of springs and spring-fed waterbodies, from the top of W7 (Table S8, sample G6). That change appears to have occurred lower in the sequence with increased influx of molluscan land taxa (both numbers of individuals and species represented) and numbers of incomplete shells (Table S7, sample G9). As there is no evidence for a concomitant increase in species representing moving water (as in channel B faunas), shrinking of the water body and a more littoral setting rather than a change in depositional environment is suggested for the upper part of W7. The thickness of W7 deposits suggests a relatively long-lived permanent pool.

Facies associations W8(WF) and W8(KD)

As both W8(WF) and W8(KD) comprise marine-influenced sediments they are potentially coeval with a limited distribution in WFQ and KDQ, although sedimentary characteristics and clast-lithology data (Fig. 6 and Table S1, C23–C26) suggest extension of W8(WF) to WF2 on the northern boundary of WFQ (Fig. S4(b)).

Infilling a channel that has cut down to bedrock Oxford Clay between W2 and W6 to the west and W3 to the east, the basal part of W8(WF) comprises vertically aggrading cut and fill gravel channels with sand–silt–clay linings at their base (Fig. 4). Clast-lithology assemblages from the lower part show derivation from W2 and W3 (Fig. 6 and Table S1, C23–C25), with the latter from below the FH in Fig. 4 containing Fe-cemented aggregates (RFH, Fig. 4), indicating that W8 post-dates the FH. An extremely fossiliferous sand ribbon (Fig. 4) representing a substantive influx of marine–brackish microfauna (facies Sm, Langford et al., in press; from sample F13, Table S9) separates this lower sequence from overlying shelly, trough cross-bedded sand and gravel. Clast-lithology (sample C26) of the

latter shows derivation from the FH, although devoid of Fe-cemented aggregates. Many of the shells in four of the six mollusc samples (F7, F9, F14 and F15, Table S9) from the lower part of W8(WF) are incomplete and Fe-stained, indicating derivation from channel B deposits. Together with the depositional characteristics, this suggests an exposed platform formed by the FH from which eroded material and slumped fine-grained bankside material were entrained into newly formed channels during the onset of flood events, prior to higher energy entrainment and slumping of bankside gravels. Sample FC2b (Table S10) records brackish–marine microfauna at the base of W8(WF), suggesting that tidal/storm surges may have been the source of some flood events. Significantly numerous well-preserved *B. marginata* are present in the molluscan assemblage of sample FC2b, whereas in most samples, they are few (Table S9) and mostly represented by fragments. Also present in the same sample, but not in the other W8(WF) samples, is the ostracod *P. olivaceus* (Table S10). Both *B. marginata* and *P. olivaceus* occur at the top of W7 (Table S6, sample G6), from which they could have been reworked into the base of W8(WF), suggesting that W8 is younger than W7. Alternatively, the presence of both species in the estuarine assemblage of mixed marine, brackish and freshwater taxa of sample FC2b could be explained by the existence of a contemporary spring on the margin of the estuary. This, however, would likely require the loss of suitable habitat in response to rising groundwater level in order to explain their apparent absence up-sequence (uncertainties in the stratigraphical order of W7 and W8 are considered in the Appendix).

Facies association W8(KD) has been dated by opercula AAG to MIS 7 (Table 2 (sample A8) and Table S4; Fig. 7(b)), has a lower notional bracketing age of MIS 8 because it overlies W4, and an upper bracketing age of MIS 6 because it underlies OSL dated W9. As reworking of the W8(KD) fauna is likely (Langford et al., in press), this facies association could date to MIS 6 or the transition from MIS 7 to MIS 6 rather than MIS 7.

Facies associations W9(WF) and W9(KD)

As W9 (WF) is overlain by W15, it has a minimum upper bracketing age of MIS 5b–a (Table 2 (samples L8 and L9) and 4). Field relationships at WF2 suggest a notional lower bracketing MIS 7 age because W9(WF) appears to cut out a northward continuation of W8(WF), an observation supported by the relatively high proportions of limestone and sandstone of sample C23 (Table S1). A shell of the temperate mollusc *B. marginata*, and the presence of the brackish ostracod *C. torosa* and foraminifera *Elphidium williamsoni*, *Elphidium macellum*, *Elphidium clavatum*, *Elphidium albiumbilicatum*, *Haynesina germanica*, the dwarfed form of *Ammonia batavus*, *Cassidulina reniformis* and *Elphidium* sp. (all found in W8(WF); Langford et al., in press) could indicate reworking of W8(WF) sediments and hence support the notional MIS 7 lower bracketing age. Although the upper bracketing age suggests that an MIS 5d–c age is possible, insect and ostracod assemblages of this age, and their respective palaeotemperature reconstructions, at nearby Tanholt Farm and Pode Hole quarries (Fig. 2; Briant et al., 2004a, 2004b, 2005) are dissimilar. As palaeoecological interpretation indicates that W9(WF) represents cold-stage conditions, a MIS 6 age is therefore suggested.

Facies association W9(KD) comprises facies Sh, PDmm and Fd and is dated by OSL to 158 ± 14 ka, that is MIS 6 (Table 2 (sample L3) and 4). As facies PDmm separates Sh and Fd, and all have experienced extensive cryogenic deformation associated with overlying W10 (Fig. S4), the exact relationship

between Sh and Fd cannot be established. Pollen analysis for facies Fd (Table S11) indicates accumulation under cool, if not fully glacial, conditions. In contrast, the ostracod and foraminifera assemblages provide a mixed palaeoenvironmental signal, suggesting incorporation of a component from earlier, more temperate deposits.

Facies associations W10(BF) and W10(KD)

Widespread in BFQ, W10(BF) has an unequivocal age of MIS 6 because it cuts out channel B (Fig. 3(a)) and is incised by channel C (W12; Fig. 3(a)), thereby providing lower MIS 7 and upper MIS 5e bracketing ages. The presence of Ca-cemented aggregates in samples C32 and C33 indicates that the indurated horizon at the top of W3 (CH and RCH, Fig. 4) pre-dates deposition of W10(BF).

Direct correlation of W10 between KDQ and BFQ, however, cannot be established on the evidence available. The 158 ± 14 ka (MIS 6) OSL date for underlying W9(KD) provides a lower bracketing age for W10(KD). An upper bracketing age is provided by the overlying W15(KD), which is associated with a later phase of cryogenic deformation (MIS 5d–2?) that post-dates reworking of reddened sands considered to be associated with a phase of temperate decalcification (MIS 5e?). The earlier intensive cryogenic deformation experienced by W9 and W10 in KDQ (Fig. S4) perhaps correlates with MIS 6 ice-wedge casts observed in W6 underlying W14 (MIS 5b–a) in WFQ, and in W2 and W3 underlying W14 in BFQ (Fig. S10), as well as in W10 underlying W12 (MIS 5e) in BFQ (junction of temporary sections B1 and C (Langford et al., 2004c, fig. 31)).

Facies association W11

Cropping out in BFQ, W11 comprises cohesive flow deposits containing pockets of fossiliferous sand and gravel, reworked from channel B (PSG, Fig. 4), which provides a lower bracketing age of MIS 7. As overlying channel C (W12) provides an upper bracketing age of early MIS 5e, and as it overlies W10(BF), W11 most likely dates to late MIS 6.

Facies association W12

Dated by opercula AAG to MIS 5e (Table 2 (sample A9) and 4; Figs. 4 and 7(b)), W12 represents deposits laid down by a northerly flowing stream in a sinuous channel under fully temperate climatic conditions. Accumulation of channel C began early in MIS 5e, as pollen data from the base indicate correspondence with Ip Ib (pre-temperate substage) of the LIG (Langford et al., 2017).

Facies association W13

Comprising a lens of horizontally stratified to planar cross-bedded, medium to fine sands (facies Sh–Sp) at the base, overlain by wavy laminated silts (facies Fl; Fig. S11), W13 contains a foraminifera fauna dominated by intertidal species, with a limited freshwater and brackish ostracod fauna also being present (Langford et al., in press). Facies Sh–Sp has been dated by OSL to 116 ± 16 ka, that is MIS 5e (Table 2 (sample L4) and 4).

Facies association W14

Comprising channel A (Fig. 3(a)) and associated overbank sediments (Fig. 4), W14 has been dated by OSL to 73 ± 4.2 to 91 ± 5.3 ka, that is MIS 5b–a (Table 2 (samples L5–L9) and 4). Although problematic because of incomplete sediment

bleaching, these dates are considered plausible due to their OSL signal being unsaturated and because of a very reliable OSL date of 77 ± 5.4 ka (Table 2 (sample L8) and 4) from immediately overlying W15. There are no published palaeoecological data for W14 but Table S12 provides a preliminary count of a restricted molluscan fauna from a sand lens in section WF1. Dominated by *Galba truncatula* (14%), *Radix* spp. (36%), *Pupilla muscorum* (15%) and Pupilidae (24%), the assemblage depicts a largely dry grassland environment with scattered pools prone to drying out (Kerney, 1999; Murton et al., 2015). The *C.* cf. *fluminalis* fragment indicates some reworking of previous interglacial deposits.

Facies association W15 and W15(KD)

Forming a widespread, cryogenically deformed, gravel sheet in WFQ and BFQ, in which lenses of reddened sand are common, W15 in WFQ has been dated by OSL to 77 ± 3.5 ka to 103 ± 5.4 ka (MIS 5b–a; Table 2 (samples L8 and L9) and 4). The younger age (L8) is considered very reliable as it has a high reproducibility D_e, indicating good bleaching prior to burial. This provides an upper bracketing age for underlying channel A (W14). The older age (L9) is considered an overestimation because of low D_e reproducibility, indicating incomplete sediment bleaching prior to burial.

Also with common lenses of reddened sand, the widespread W15(KD) in KDQ has a lower bracketing age of MIS 6 because it overlies W9(KD) dated by OSL to 158 ± 14 ka. In section KD2, deposition accompanied cryogenic deformation that post-dates reworking of reddened sands attributed to temperate climate weathering. Ice-wedge casting is also evident at section KD1 (Fig. S12), but this could be post-W15(KD).

Facies association W16

Forming a broad gravel sheet at the western end of BFQ, W16 cuts out W10 and W12 and, in turn, is overlain by W17 and W18. It therefore has a maximum lower bracketing age of MIS 5e. Deposits of W16 have not been described so far, but ice-wedge casts truncated by W17 have been observed. Part of a horse jaw, complete with teeth, has been found (Figs. 4(c) and S13) at the top of W16, suggesting a minimum age of MIS 3 (Pin Hole mammalian assemblage, Currant and Jacobi, 2001), which is confirmed by OSL dating (41.6 ± 4.3 to 44.6 ± 4.2 ka; Table 2 (samples L10 and L11) and 4).

Facies association W17

Structureless muds of channel D1 and the major sand-bed stream deposits of channel D2 (Fig. S14) comprise W17, which has an upper bracketing age of MIS 2 as it underlies W18. It is incised into W16 in the western part of BFQ, indicating a lower bracketing age of MIS 3. Woolly rhinoceros bones from channel D1 muds suggest an age of MIS 3 (i.e. Pin Hole mammalian assemblage, Currant and Jacobi, 2001), which is confirmed by radiocarbon ages of ca. 50 000–40 000 years BP on a woolly rhinoceros bone and plant seeds from channel D1 (Tables 2 (samples R1–R3) and 5), comparable to the 48.8–37.3 ka age range of the OSL dates for underlying W16.

Facies association W18

Extensive sheets of pebbly gravel were observed to overlie channel D1 on the northern and southern boundaries in the western part of BFQ. No data are available for these deposits of W18, but as they are underlain by channel D1 and overlain by Holocene Peat, they have lower and upper bracketing ages of

MIS 3 and MIS 1, respectively. Extensive pebbly gravel sheets observed in MFQ (Fig. 3(b)) beneath the MIS 1 sequence depicted in Fig. 5 were assumed to represent W18. An MIS 2 age of 14.7 ± 1.04 ka for W18 at section MF2 in MFQ (Table 2 (sample L12) and 4; Figs. 3(b), 5 and 8; Fig. S15) was obtained by OSL. However, as there is no lower bracketing age (other than MIS 3) from the evidence available, other lower parts of W18 could be older than the OSL age.

Facies association W19

This facies association represents the development of soil on W18 gravels, followed by the accumulation of silts and the development of the Lower Peat. Published radiocarbon ages for the Lower Peat of the area are 5090 ± 30 and 4735 ± 30 years BP (Table 2 (samples R4 and R5) and 6; Fig. 9).

Facies association W20

Facies association W20 represents tidal creek deposits infilling a channel that is incised through the Barroway Drove Beds and W19 into the underlying gravels of W18, in turn overlain by a later freshwater channel and Nordelph Peat. An age of 5345 ± 30 years BP (Table 2 (sample R6) and 6) was reported for the earliest tidal creek (rodden; channel F, Fig. 9) and an age of 3687 ± 35 years BP (Table 2 (sample R7) and 6) was reported for the later freshwater tributary of the River Nene (channel G, Figs. 3(b) and 5). The base of channel G dates to about 3250 years BP and the top to about 2050 years BP, and the Nordelph Peat started forming in the area from 3645 ± 30 to 2090 ± 30 years BP (Table 2 (samples R8–R11) and 6). Knight and Brudenwell (2020) have dated archaeological material that records the rise of the fen edge in BFQ as human occupation translocated upwards, from 0 m OD at 4150–3900 years BP to 1.5 m OD at 2330–2130 years BP (Table 6; Fig. 9). For this study, an OSL sample was collected from section MF2 in order to date the Barroway Drove Beds of W20 (Figs. 3(b), 5 and S19). Unfortunately, the OSL age of 14.6 ± 0.87 ka (Table 2 (sample L13) and 4; Fig. 8) corresponds to MIS 2 and is therefore problematic; either the Nordelph Peat lies directly on MIS 3–2 overbank fines, as appears to be the case in sections BF1 and BF2 in BFQ, or the dated sediments are derived from underlying W18. As the Barroway Drove Beds of section MF2 can be traced to section MF1, where they overlie Lower Peat deposits (Smith et al., 2012), derivation from underlying W18 is most probable. Thus, the OSL dating proved unreliable because the 14 ka date does not reflect the MIS 1 age of the Barroway Drove Beds. Although the age of the heterolithic Barroway Drove Beds in MFQ remains enigmatic, they probably represent the overbank deposits of channels F and G.

Discussion

Table 7 demonstrates the robust geochronology of the WSS: grey shading indicates those facies associations that have been dated numerically (by AAG or luminescence or radiocarbon, column 5) and also where they provide bracketing ages (columns 4 and 7); facies associations with direct evidence of temperate or cool/cold conditions are also highlighted (column 6); previous nomenclature for a particular facies association (or part of) is given in brackets [], as opposed to parentheses () (column 1). Fig. 10 synthesises the available information and makes a comparison with the global record (Lisiecki and Raymo, 2005).

The journey so far

Site stratigraphy (Tables 3 and 7; Figs. 4, 5, 10 and S4–S6) indicates that the WSS commenced with incision and infilling of a channel trending NE–SW under cold conditions, as testified by the presence of *Leucocythere batesi* and the exotic cold-indicator coleopteran species *Helophorus obscurellus*, *Helophorus* cf. *orientalis*, *Tachinus furcatus* and *Otiorhynchus politus* (Langford et al., 2014b); the latter suggests cold, dry continental climatic conditions. It is important to note here that several cold-indicator coleopteran species identified in numerous British MIS 5d–2 contexts are present in W1, W3(WF) and W9(WF), thus limiting their biostratigraphic utility. Palaeotemperature reconstruction indicates mean air temperature between −32°C and +9°C for the coldest month and between +13°C and +19°C for the warmest month (by consensus of beetle and ostracod proxy methods; Langford et al., 2014b). Flow direction was to the northeast and clast-lithology data indicate primarily local derivation from Anglian flint-rich deposits to the west (Fig. 2). Subsequent deposition of the gravel sheets of W2 testifies to flow expansion in a braided (multithread) stream flowing to the north to east quadrant. The presence of boulder-size organic mud clasts, as in W1, suggests accumulation under the same cold-climate regime. Clast-lithology data indicate an increased flux of Middle Jurassic limestone, suggesting upstream drainage network extension towards the west (Langford et al., 2004b). Incision by a relatively sandstone-rich gravel-bed stream (W3) under moderately cold-climate conditions followed (Langford et al., 2007), with consensus reconstructed mean monthly palaeotemperature ranges of between −8°C and −3°C for the coldest month and between +12°C and +14°C for the warmest month (Langford et al., 2014b). Of the exotic cold-indicator species present amongst the WSS coleopteran fauna, *Olophrum boreale*, *Philonthus linki* and *Hippodamia arctica* are exclusive to W3(WF). Flow in BFQ was to the southeast, changing to north of east in WFQ. The increased flux of sandstone clasts could testify to westward fluvial extension, either as part of glacial-meltwater-generated flows through the upstream Southorpe dry valley (Fig. 10; Langford, 2018) or influx of Permo-Triassic bedrock erosion in the English Midlands, or to deeper erosion of local Anglian deposits or erosion of local interfluves to the west. Widespread limestone-rich (cf. W2) gravel sheets (W4) in KDQ again indicate flow expansion with flow direction to the north to east quadrant (Langford, 1999). High proportions of Middle Jurassic limestones at the expense of flint and sandstone could suggest reduction of the drainage network (cf. W3) to the middle–lower Nene catchment and deposition from floodwaters (rather than the multiple recycling under normal flow conditions that increases clast comminution potential) to explain the limestone enrichment, perhaps as a result of breaching of an alluvial–delta fan complex at the upstream confluence of the Nene and Southorpe dry valley (Fig. 10; Langford, 2018).

Channel B (W5 and W6) represents a northeastward flowing, gravel-bed, sinuous single-thread stream with associated heterolithic overbank deposits that provided a habitat suitable for exotic thermophile molluscs *B. marginata*, *C.* cf. *fluminalis* and *T. danubialis* (Langford et al., 2014a). Pollen from the basal muddy gravel and abandoned channel infill indicated accumulation of channel B in the late temperate
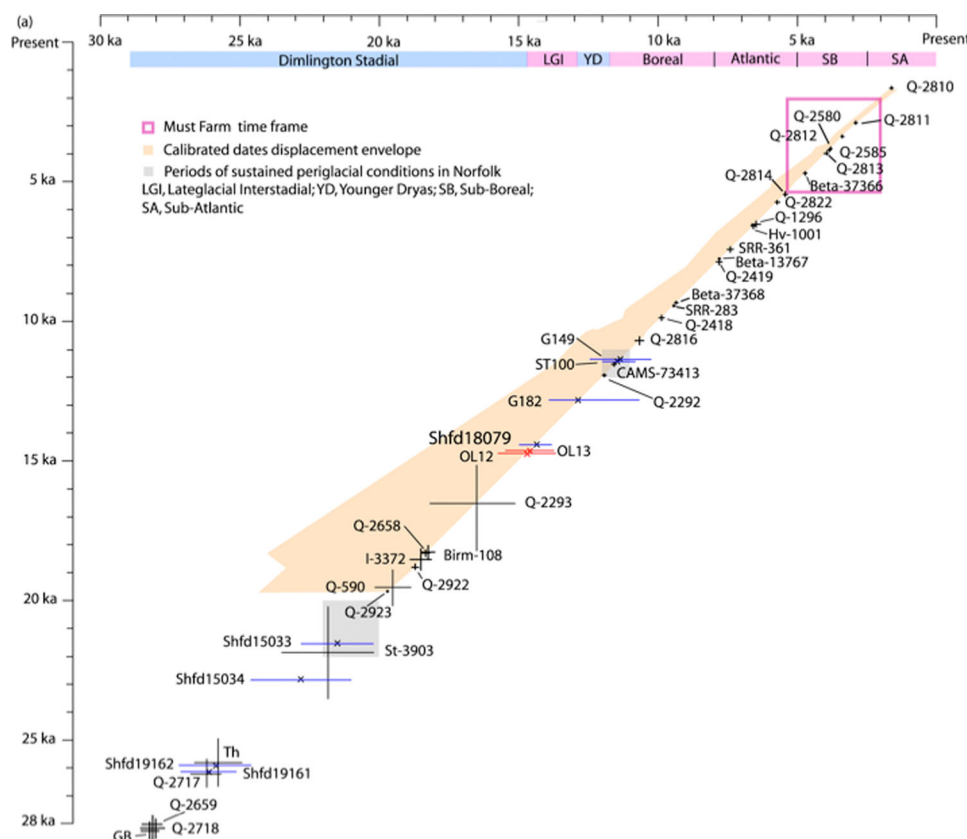
Figure 8. Lateglacial Interstadial OSL dates for facies associations W18 and W20 in MFQ plotted alongside published MIS 2 and MIS 1 dates (Morgan, 1969; Holyoak and Seddon, 1984; West, 1991, 1993; Waller, 1994*; West et al., 1999*; Briant et al., 2004d*, 2008*; Scaiffe, 2004*; Smith et al., 2012*; Bateman et al., 2014; Roberts et al., 2018; Gibbard et al., 2021). See Fig. 9 for data on the Must Farm time frame. *Sources of calibrated radiocarbon dates used for constructing the displacement envelope. [Color figure can be viewed at wileyonlinelibrary.com]

substage of an interglacial stage. Beetle and ostracod consensus palaeotemperature reconstruction indicates mean air temperature between −1°C and 3°C for the coldest month and between +16°C and +21°C for the warmest month (Langford et al., 2014a). Post-depositional weathering at the top of W6 gravels pre-dates W7 and W8 and suggests a significant post-channel-B hiatus, following which molluscan fauna indicate accumulation of W7 in a low-energy, high-water-table environment, with a fall in water table at the top providing a habitat suitable for spring-dwelling molluscs and ostracods. Incision and episodic infilling of a channel trending NE–SW are recorded by W8(WF), with an influx of estuarine–marine microfauna indicating a maximum sea-level approximation of <0.5 m OD. This is an important record because prior to Bateman et al. (2020) and Langford et al. (in press), there were no reliably dated attributions to the penultimate interglacial sea level for Fenland. Gravel-bar-top reworking and subsequent development of a shallow, clear freshwater pool with an influx of estuarine–marine taxa by an easterly flowing stream are recorded by W8(KD) (Langford, 1999). As the estuarine–marine taxa are considered to be reworked from earlier MIS 7 deposits (Langford et al., in press), they do not provide a meaningful sea-level approximation.

At least two major incisional events are recorded by W9(WF) from about 1.5 m to about −3 m OD, forming channels trending NE–SW, each episodically filled with organic gravel and mud under cold-climate conditions (Langford et al., 2014b). Consensus palaeotemperature reconstruction ranges are between −8°C and −2°C for the coldest month and between +11°C and +16°C for the warmest month (Langford et al., 2014b). Of significance is the presence of four cold-indicator ostracod species (*Fabaeformiscandona levanderi*, *Limnocythere sanctipatricii*,

Table 5. Published radiocarbon age estimates for channel D1 (W17).

FA	Quarry	Sample	Comments
W17	BF	R3	*Coelodonta antiquitatis* bone: OxA-31962 40 400 ± 1200 yr BP (uncalibrated) 43 787–40 400 cal. yr BP (95.4%)
W17	BF	R2	*Potamogeton*: OxA-X-2629-39 45 200 ± 1100 yr BP (uncalibrated, beyond calibration range)
W17	BF	R1	*Carex*: OxA-X-2627-56 40 300 ± 2700 BP (uncalibrated) 49 892–41 512 cal. yr BP (95.4%)

Source: Briant et al. (2018).

Juxilyocypris schwarzbachi and *Amplocypris tonnensis*) in addition to the extinct *L. batesi*. Of the exotic cold-indicator coleopteran species, *Helophorus splendidus* and *Boreaphilus henningianus* are exclusive to W9(WF). Coeval accumulation with W9(KD) at different topographic levels on a braid plain is plausible (Miall, 1977), but similar changes in facies architecture within the last glacial were ascribed to climatic forcing by Briant et al. (2004a, 2004b, 2005) at nearby Tanholt Farm and Pode Hole quarries (Fig. 2), where the lower channelised facies yielded palaeotemperature estimates slightly colder than here at WSS, but still milder than during deposition of the largely horizontally bedded upper facies. Aggradation of W9(WF) is considered to have preceded W9(KD) because the latter dates to the second half of MIS 6, prior to the accumulation of W10, leaving little opportunity for a subsequent incision and infilling phase late in MIS 6

Table 6. Published radiocarbon age estimates for facies associations (FA) W19 and W20 in Must Farm Quarry.

FA	Holocene sequence[a]		Bradley Fen fen-edge migration[b]	
	Sample reference	Deposit (years BP, i.e. before 1950)	m OD	Years BP (i.e. before 1950)
W20	R10, R11	Nordelph Peat 3645 ± 30/2090 ± 30	1.5	2330–2130
	R9	Top of freshwater channel 2050	1	2690–2340
	R8	Base of freshwater channel 3250	0.5	3140–2880
	R7	Maximum age of freshwater channel 3687 ± 35 on mollusc	~0.25	3570–3340
	R6	Maximum age of roddon 5345 ± 30 on foraminifera	0	4150–3900
W19	R4, R5	Latest (Lower Peat) phase 5090 ± 30/4735 ± 30		

[a]Smith et al. (2012).
[b]Knight and Brudenwell (2020).

(see below). The deposits of W9(KD) represent a single thread, sand-bed stream flowing towards the northeast, followed by bank collapse and muddy organic infilling of a shallow pool that pollen indicates accumulated under cool, if not cold, conditions (Langford et al., 2004a). The sands and muds of W9(KD) were severely cryoturbated following deposition of W10(KD) gravels (Langford, 1999), believed to be related to W10(BF). The southerly flow indicated by the deposits of W10(BF) probably represents drainage diversion in response to downstream glacial impoundment at The Wash (Fig. 10) at about 141 ka (Evans et al., 2019). Ice-wedge casting was observed beneath overbank fines of channel C (W12), possibly correlated with the large-scale cryoturbation of W10(KD). Subsequent left-bank collapse of the southerly flowing, gravel-bed braided river led to the cohesive-flow deposits of W11 that contained fragments of *C.* cf. *fluminalis* and *T. danubialis* reworked from W6 (Langford et al., 2017).

Pollen data from the basal muddy gravels of the sinuous, northward-flowing, single-thread channel C demonstrate that drainage reversal following W10(BF) diversion had occurred by Ip Ib (pre-temperate substage) of the LIG (Langford et al., 2017). The presence of exotic thermophiles *Naias minor*, *B. marginata*, *Bembidion elongatum*, *Pelochares versicolor*, *Caccobius schreberi*, *Onthophagus massai* and *Emys orbicularis*, usually associated with Ip IIb (early temperate substage) of the British LIG record, accords with global records of rapid climate amelioration. Consensus palaeotemperature reconstruction shows mean air temperature between 0°C and +7°C for the coldest month and between +19°C and +22°C for the warmest month (at least 2°C warmer than present) when the basal muddy gravel was deposited (Langford et al., 2017). Uniquely, *Herpetocypris helenae* is present amongst the ostracod fauna, the only identification of it so far in the Pleistocene fossil record. At about 116 ka, an influx of estuarine–marine foraminifera in W13 indicates a maximum sea-level approximation of <3 m OD, which is one of only two reliably dated LIG sea-level records for Fenland (Langford et al., in press).

About 90 ka, a major single-thread gravel-bed river with extensive heterolithic deposits on its left bank (W14) flowed to the northeast in WFQ and more easterly in KDQ (Langford et al., 2007). This was succeeded by flow expansion through shallow braided streams and deposition of extensive gravel sheets (W15) in BFQ, KDQ and WFQ at about 77 ka, with extensive post-depositional cryogenic deformation evident in KDQ and WFQ, as well as minor synformational cryogenic deformation in KDQ (Langford, 1999). Nodular chalk is persistently present in the clast-lithology counts of W14 and W15, suggestive of slope erosion of local interfluves mantled by Anglian chalk-rich diamictons. Preservation of these clasts suggests relatively short-lived transport between erosion and burial, perhaps by episodic floods. Westward in BFQ, a broad gravel sheet (W16) with a minimum age of about 43 ka (Briant

et al., 2018) cuts out W10 and W12, and has experienced ice-wedge casting and yielded a horse jaw-bone complete with teeth. Overlying, single-thread, muddy channel D1 (W17), with a northward-descending thalweg that suggests flow to the north, is of similar age. Palaeotemperature reconstructions suggest fluctuating mean-air-temperature regimes during accumulation, and hence episodic infilling (Langford et al., 2014b). Deposits of the shallow, braided sand-bed channel D2 (also W17) that interdigitate with those of the upper part of channel D1 suggest a flow direction of west of north. A subsequent higher-energy, braided flow regime deposited the widespread gravel sheets of W18 in BFQ and MFQ. Brief observations of temporary exposures in MFQ suggest an easterly flow direction for W18, which has a minimum age of ≤15 ka.

There appears to have been a hiatus of several thousand years following Pleistocene aggradation in MFQ, as the soil horizon at the base of W19 probably represents the period from 6 to 4.5 ka when locally large areas were relatively dry (Knight et al., 2024). The Lower Peat at the top of W19 marks the change to wetter conditions at <5 ka, coincident with the formation of channel F (sinuous, single-thread tidal creek) and transition to deposition of W20. Subtidal conditions were short-lived in channel F, perhaps less than a decade, transitioning to intertidal conditions (Smith et al., 2012). Freshwater, sinuous single-thread channel G (W20) developed in three phases encompassing the late Bronze Age to late Iron Age (Knight et al., 2024), with the Must Farm pile-dwelling settlement and abandonment near the end of the first phase, when it was up to 25 m wide and 3 m deep. A period of channel widening to 35 m ensued, followed by narrowing to <16 m wide and shallowing to no more than 2 m deep, prior to transition to Nordelph Peat about 2 ka.

The onward journey

As apparent from Table 1 there are several alternative stratigraphic interpretations of River Nene fluvial deposits, none of which accurately reflect the morphology and aggradation pattern of the WSS. Rather than critically evaluate and compare these contrasting views, our objective here is to embrace the advances that have been made (e.g. constraints on past ice limits, drainage reorganisation and sea level; Fig. 10) and to shine the light forward. Thus, the WSS record outlined here is envisaged as a framework/informal database for future research, or as the basis of a formal database to be developed for the provision of a comprehensive Quaternary history of palaeoenvironmental conditions experienced at a place (i.e. the WSS) near the edge of the ice or sea at the respective extremes of the past three glacial–interglacial cycles. As a database, the WSS has the advantage of being securely dated, capable of being added to incrementally as

Table 7. Numerically dated facies associations and their lower and upper bracketing roles.

Previous studies	This study	Other underlying*	Lower bracketing‡	Facies association†	PC	Upper bracketing‡	Other overlying*
Smith et al. (2012)	Section MF1 (Figs. 3(b) and 5)		W19	W20[14C] (Channel F)	tan	W20	
Smith et al. (2012)	Section MF1 (Figs. 3(b) and 5)	OxC	W18	W19[14C] (Channel E)	blue	W19	
Langford et al. (2004c[channel D], 2014b [unit 5d])	Sections BF1 and BF2, Figs. 3(b), S4(c), S5(d) (iii) and S6(a)	W10(BF)	W17	W18[OSL]	blue	W18	Holocene
Langford et al. (2014b [unit 5c])	Sections BF1 and BF2, Figs. 3(b), S4(c), S5(d) (iii) and S6(a)	OxF	W16	W17[14C] (Channel D)	blue	W17	
Langford (1999 [A5]), Langford et al. (2004a1844)	Sections KD1–KD3, Figs. 3(a), S4(a), S5(d) (ii) and S6(b)	W4	W10(BF)	W16[OSL]	blue		
Langford et al. (2004b[unit 6], 2007 [unit F6])	Sections WF1–WF5 and BF5, Figs. 3(b), S4(b),S4(c), S5(d) (ii) and S6(a)	OxC/W6/W7/ W8(WF)/W9(WF)	W10(KD)	W15(KD)		W15	
Langford et al. (2004b[units 5a and b], 2007 [units F5 and G4])	Sections WF1–WF5 and BF5, Figs. 3b, S4(b) and S4(c), S5(d) (i) and S6(a)	OxC/W3/W6	W14	W15[OSL]		W15	
Langford et al. (2004a)	Section KD4, Figs. 3(a), S4(a), S5(b) and S6(b)		W8	W14[OSL] (Channel A)	tan		
		OxF/W10(BF)	W4	W13[OSL]		Holocene	
Langford et al. (2004c [channel C], 2017 [units 4a and b])	Section BF5, Figs. 3(b) S4(c), S5(b) and S6(a)		W11	W12[AAG] (Channel C)	blue	W12	Holocene
Langford et al. (2004c [Channel E], (2017) [unit 3c])	Section BF4, Figs. 3(b), S4(c), S5(c) (iii)	W3	W10(BF)	W11[RW5]	blue	W15(KD)	W12/W17
Langford (1999 [A4]) and Langford et al. (2004a)	Sections, KD1 and 2, Figs. 3(a), S4(a), S5(c) (ii) and S6(b)	W4	W9(KD)	W10(KD)		W11	
Langford et al. (2004c [unit 7 and part of unit 2], 2017 [unit 3b])	Section BF3, Figs. 3(b), S4(c), S5(ii) and S6(a)	W2	W3[Indurated(Ca)]	W10(BF)[RW4]	blue	W10(KD)	
Langford (1999) and Langford et al. (2004a) [Facies Sh, Sd, Fd and PDmm]	Section KD2, Figs. 3(a), S4(a), S5(c) (i) and S6(b)		W8(KD)	W9(KD)[OSL]		W10(KD)	
Langford et al. (2014b [unit 3a])	Section WF2, Figs. 3(b), S4(a), S4(b) and S6(c) (i)	OxC	W8(WF)[RW3]	W9(WF)	tan	W15	
Langford (1999) and Langford et al. (2004a) [Facies PGcs and Fl–Fm]	Section KD2, Figs. 3(a), S4(a), S5(b) and S6(b)		W4	W8(KD)[AAG]	tan	W9(KD)	
Langford et al. (2004b [units 4a (part of) and 4b], 2007 [units F2 and F3])	Section WF3, Figs. 3(b), S4(b), S5(b) and S6(a)	OxC/W3/W6	W7[RW2,3]	W8(WF)[AAG]	tan	W15	
Langford et al. (2004b [unit 3f])	Sections WF4, WF5 and BF5, Figs. 3(b), S4(b), S4(c), S5(b) and S6(a)		W6[Indurated (Fe)]	W7[AAG]	tan	W8(WF)[RW3]	W14/W15
Langford et al. (2004b [units 3c–e])	Sections WF3–WF5 and BF5, Figs. 3(b), S4(b), S4(c), S5(b) and S6(a)	OxC/W2	W5	W6[AAG] (Channel B)		W7	W8(WF)/W14/W15
Langford et al. (2004b [units 3a and3b], 2014a [unit 2a])	Sections WF4 and WF5, Figs. 3(b), S4(b), S5(b) and S6(a)	OxC	W2	W5[AAG] (Channel B)		W6	W10(KD)/W13/ W15(KD)
Langford (1999 [1a]), Langford et al. (2004a [1a])	Sections KD1–KD4, Figs. 3(a), S4(a), S5(a) (iv) and S6(b)	OxC	OxC	W4[AAG]		W8(KD)	
Langford et al. (2004b [unit 4a], 2007 [unit F1], 2014b	Sections WF3 and BF4, Figs. 3(b), S4(a), S5(a) (iii) and S6(a)	OxC	W2	W3[AAG]	blue	W8(WF)	W10(BF)/W11/W14

(Continued)

Table 7. (Continued)

Previous studies	This study	Other underlying*	Lower bracketing‡	Facies association†	PC	Upper bracketing‡	Other overlying*
[unit 1cl]							
Langford et al. (2004b [unit 2], 2007 [unit G1], 2014a [unit 1bl])	Sections WF3–WF5 and BF5, Figs. 3(b), S4(b), S4(c), S5(a) (ii) and S6(a)	OxC	W1	W2^RW1		W3	W5/W6
Langford et al. (2004b [unit 1], 2014b [unit 1al])	Sections WF4 and 5, Figs. 3(b), S4(b), S5(a) (i) and S6(a)	OxC	Anglian^CL	W1^RW1	[greyshade]	W2	

*The relevant facies association also directly underlies/overlies these facies associations/bedrock in places.
‡Greyshade indicates that numerically dated bracketing facies association is in viable stratigraphical order.
†Greyshade indicates dated numerically.
PC, palaeoclimatic conditions indicated by palaeoecological/palaeotemperature analyses or observed cryogenic deformation: pink shading, fully temperate; blue shading, cool/cold; OxC, bedrock Jurassic Oxford Clay.
AAGDated by amino acid geochronology; OSLDated by optically stimulated luminescence; 14CDated by carbon-14.
CLClast-lithology determinant: presence of flint, introduced into the area from the northeast during the Anglian glaciation.
Indurated(Fe)Post-depositional Fe-cemented indurated horizon formed between W6 and W8; Indurated(Ca)Post-depositional Ca-cemented indurated horizon formed between W3 in BFQ and W10(BF). RW1Reworked boulder-size clasts of stratified organic muds; RW2reworked clasts of Fe-cemented indurated horizon; RW3reworked clasts of Ca-cemented indurated horizon; RW4reworked W7 fossil fauna; RW5sand and gravel pockets containing reworked channel B molluscs.

research methods and knowledge improve, and resilient and relevant for answering important questions concerning climate and sea-level change, both locally and regionally. Looking forward, the incomplete and empty spaces are just as relevant as those that have been filled.

The value of having such a database is that it can be dated directly, whereas global reconstructions from deep-sea and ice-core records largely depend on tuning to various age models or absolute-dated sequences. Long terrestrial records comparable to marine and polar ice records are rare, and well-dated ones even more so (Giaccio et al., 2024). Under these circumstances, it would therefore seem sensible to group together well-dated shorter terrestrial sequences over a limited area, and to incorporate reliably dated information from nearby deposits to augment and extend the record of fragmentary fluvial sequences. Detailed palaeoecological data within such terrestrial records would be valuable for: contributing towards a global terrestrial palaeotemperature database (Kaufman et al., 2020); testing regional synchroneity or otherwise of global palaeoclimate reconstructions from long marine and polar ice records (Westerhold et al., 2024); establishing authentic habitat suitability for flora and fauna prior to anthropogenic ecological changes (Mills et al., 2024); tracking biodiversity; identifying local-scale differences and dynamics in habitat structure; examining local versus regional factors determining habitat structure; challenging the orthodoxy of established paradigms (Pearce et al., 2025). The BRITICE project (Clark et al., 2018) is a recent successful example of dedicated research using such a multifaceted approach, and the World Atlas of Last Interglacial Shorelines (WALIS) is an example of ongoing development of a database (Cohen et al., 2022) similar to that envisioned here.

Development of the database should be possible through: (i) addressing the uncertainties recognised in the Results section; (ii) expanding the multidisciplinary approach; (iii) extending and expanding the database to include nearby and Fenland-wide Quaternary deposits; (iv) applying new and improved research techniques.

Future investigation of the WSS

Some of the issues identified in the Results section can be addressed in the immediate future. For example, through luminescence dating of currently unprocessed samples, there is potential for MIS 7 tie-point dating from W6 and better age control should be possible for W15 (MIS 5b–5a) and W17 (MIS 3) deposits: from a sand lens in overbank deposits of channel A at section BF5; a non-deformed sand lens in W15 at section WF4; from the sandy facies of channel D2 at section BF1 (Figs. 3 and S4). Further insight also could be gained from additional palaeoecological analyses: an ostracod fauna from W4 at section KD3; molluscan and ostracod faunas from W5 to W8 in WFQ (see the Appendix); molluscan faunas from W9 and W14 in WFQ, and the point-bar facies in W12 in BFQ; ostracod faunas from channel D1 at section BF2. Such in-depth palaeoecological research could, for example, identify distinctive MIS 7 faunas, perhaps representing separate climatic substages, and could, in particular, facilitate a comprehensive palaeotemperature reconstruction based on the Mutual Ostracod Temperature Range (MOTR) method (Horne, 2007; Horne and Mesquita, 2008; Horne et al., 2012). Other issues, such as refining the ages of W1–W4 and distinguishing the MIS 3 heterolithic overbank deposits of W17 from those of the MIS 1 Barroway Drove Beds (W20), would require new research, including further fieldwork and sediment sampling.

There is scope to enhance the WSS database through additional proxy palaeotemperature data other than coleopter-

10991417, 0, Downloaded from https://onlinelibrary.wiley.com/doi/10.1002/jqs.70033 by Open Access Sheffield - UNIVERSITY OF SHEFFIELD , Wiley Online Library on [16/12/2025]. See the Terms and Conditions (https://onlinelibrary.wiley.com/terms-and-conditions) on Wiley Online Library for rules of use; OA articles are governed by the applicable Creative Commons License

an and ostracod mutual climatic/temperature ranges, as for example by Tye et al. (2016), Langford et al. (2017), Kaufman et al. (2020), Horne et al. (2023), Krahn et al. (2024) and Rigterink et al. (2024). Trace element (Mg, Sr) and stable isotope ($^{18}O/^{16}O$, $^{13}C/^{12}C$) determinations applied to ostracod shells could provide further palaeotemperature and palaeoenvironmental insights (Holmes and De Deckker, 2017). An interesting observation from the preliminary trace-element determinations on *C. torosa* shells from W5 is that the inferred low-salinity water may be inconsistent with the fact that the *C. torosa* shells were non-noded forms, which usually are found in more saline water (J. Holmes, personal communication, 2025). This inconsistency could be examined further using material from the WSS and making a comparison with material from marine-influenced deposits at Northam Pit (Eye) and Fore Fen Quarry (Somersham), both comparable in age to channel B (Langford et al., in press). Additional dating techniques also could be applied, such as luminescence dating of *B. tentaculata* opercula (Duller et al., 2015; Duller and Roberts, 2018, 2024; Colarossi et al., 2025) and AAG dating of ostracods (Ortiz et al., 2013; De Santis et al., 2018). The comprehensive opercula AAG dating of the WSS should provide reliable tie points for the application of either technique. Depending on its successful development and its resolution, opercula luminescence dating could resolve stratigraphic uncertainties at the climatic substage level, particularly within MIS 7, where different warm substages were of similar amplitude (e.g. those considered in the Appendix). It could also determine the age of onset of the LIG in lowland Britain if opercula from W12 were dated, and together with the luminescence dating of W13, provide an idea of the duration of the LIG fully temperate conditions in Britain. This is of regional importance because of the discordance in LIG duration between northwestern and southern Europe, of about 1500–3000 years (Lauterbach et al., 2024), as well as the dates of LIG inception and peak relative sea level regionally and globally (Sier et al., 2015).

Beyond the WSS

The WSS database could be extended to include the nearby Hoxnian Woodston Beds, but this may not be straightforward, because here, as at WSS, recent research has suggested the preservation at the same altitude of deposits of markedly different ages. The Hoxnian Interglacial is widely regarded as being equivalent to MIS 11 (Bowen, 1999) or at least MIS 11c (Horne et al., 2023), and compatibility of the Woodston Beds with MIS 11 has been demonstrated by IcPD dating (Penkman et al., 2011, 2013) and mammal biostratigraphy (Schreve, 2001). Previously, however, material from the Woodston Beds had been dated by the A/I technique to MIS 9 (Horton et al., 1992), therefore the possibility arises that they have both MIS 11 and MIS 9 components. This same possibility also arises for the downstream Hoxnian Nar Valley Beds, which have recently been dated to MIS 11, but with a suggestion of an MIS 9 component (Barlow et al., 2017). Similarly, as J. Hollin (personal communication, 1998) suspected, Holsteinian deposits in Germany would appear to be a conflation of two separate interglacials (Urban, 1995; Geyh and Müller, 2005; Meijer and Cleveringa, 2009; Stephan, 2014; Schaumann et al., 2021), which recently has been confirmed for superposed interglacial deposits at Schöningen, with the upper Reinsdorf sequence being ascribed to MIS 9 and the lower sequence to MIS 11 (Krahn et al., 2021, 2024). This is of relevance for the WSS because the mean A/I ratio of 0.25 for W4(KD) suggests compatibility with Holsteinian deposits at Wacken in Germany (Miller and

Mangerud, 1985; Fig. 7(e), and assigning the reworked *A. goodalli* and *B. tentaculata* opercula of W3(WF) and *Littorina* of W4(KD) to MIS 9 would present a problem if the only known source material is dated to MIS 11.

Expanding the WSS Fenland-wide would undoubtedly enable gap-filling of the record from the past three glacial–interglacial cycles. Complex late Quaternary deposits are not uncommon within Fenland (West et al., 1999; Boreham et al., 2010), but their stratigraphical interpretation is not straightforward because, for example, of insufficient reliable dating or reliance on pollen stratigraphy. Earlier *Corbicula*-bearing, marine-influenced deposits associated with later marine-influenced deposits devoid of *Corbicula* at Block Fen, Somersham and Wretton (Sparks and West, 1970; West et al., 1995, 1999) raise the possibility of separate MIS 7 and MIS 5e high relative sea-level (RSL) events, as do the marine-influenced deposits of W8(WF) and W13 (Langford et al., in press). There is therefore considerable potential that adequately dated, future multidisciplinary research of these deposits would enable the WSS database to become a wider Fenland database. Although important palaeoenvironmental data for W12 have been published (Langford et al., 2017), and these data, along with data from Deeping St James, have contributed to questioning the validity of the interglacial full forest canopy paradigm (Pearce et al., 2025), well-dated late temperate forest (IpIII) data are absent from the WSS and rare for Fenland as a whole (Langford et al., in press). Such data could provide valuable supporting information for W13 and insight into Fenland peak RSL extent during the LIG.
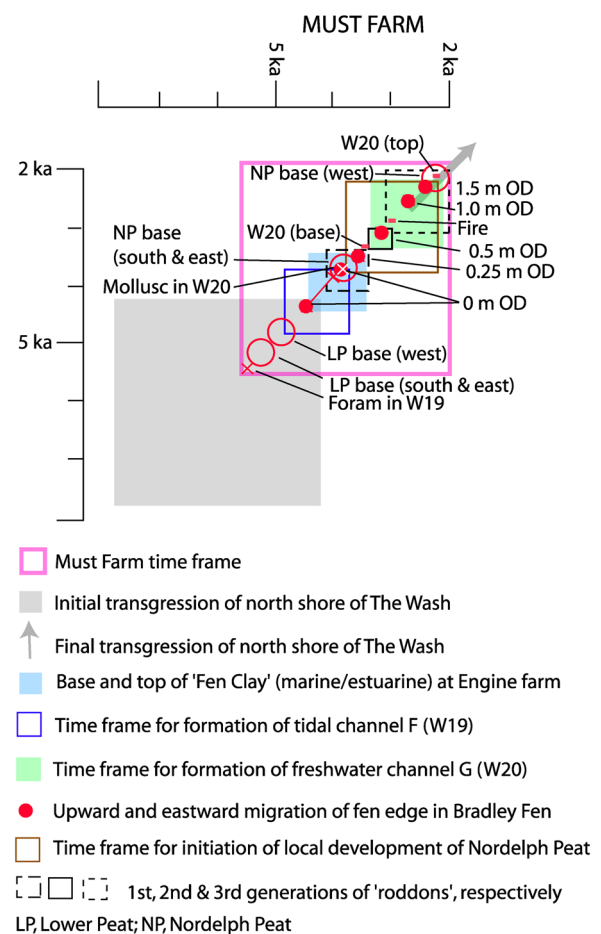

Figure 9. Radiocarbon dates and age ranges for facies associations W19 and W20 in MFQ reported by Smith et al. (2012) and Knight and Brudenwell (2020), with additional data from Waller (2004) and Brew et al. (2015). [Color figure can be viewed at wileyonlinelibrary.com]

Recent research has started to fill in the age-estimate gaps of the depositional record of the River Nene for MIS 5d–2, although for the WSS there is currently a lack of information for MIS 5d, 5c, 4 and 2. At nearby Pode Hole Quarry (Fig. 2; Briant et al., 2005; Briant and Bateman, 2009) OSL dates of 121 ± 10 to 106.2 ± 9.8 ka indicate accumulation spanning MIS 5d, at 31.3 ± 2.1 ka towards the end of MIS 3 and 10.5 ± 1.2 ka at the MIS 2–1 transition. At nearby Tanholt Farm (Fig. 2), OSL dates of 122.9 ± 6.4 to 44.6 ± 3.1 ka (Briant et al., 2004a; Briant and Bateman, 2009) indicate a more complex aggradation pattern extending to the start of MIS 3, which is the maximum age for the presence of woolly rhinoceros and horse (Chancellor and Langford, 1992). Extension of accumulation to MIS 2 could be indicated by the $24\,295 \pm 260$ yr BP ^{14}C date on mammoth tusk, but contamination of the dated material raises questions about the reliability of this date (Bateman, 1999). Further afield at Deeping St James in the River Welland catchment (Fig. 1), OSL dates of 104.6 ± 6.18 to 32.57 ± 4.07 ka also indicate complex aggradation spanning MIS 5c to MIS 3 (Keen et al., 1999; Briant et al., 2004c).

Holyoak and Seddon (1984) noted the lack of deposits in the region reliably dated to 25–10 ka, and Briant et al. (2005) also noted a lack of deposits reliably dated to the Last Glacial Maximum (LGM; about 30–15 ka). These observations extend to the Nene catchment as a whole and to Fenland, including the WSS, but as Fig. 8 demonstrates, recent research is starting to fill in the gaps. At Watlington, Gibbard et al. (2021) provide evidence of severe cryogenic conditions at 26.1 ± 1 and 25.9 ± 1.3 ka, prior to

ice impinging on the north Norfolk coast at 22.8 ± 1.8 to 21.5 ± 1.3 ka (Roberts et al., 2018). At Somersham, Lake Sparks has a calibrated ^{14}C age of 24 030–20 080 yr BP (West, 1993), coincident with ice impingement on the north Norfolk coast. Lake Sparks endured for a minimum of 65 years and had a surface level at no more than 1 m OD. There is no evidence so far for associated lacustrine deposits elsewhere in Fenland, although the lake may have extended to The Wash (Brew, 1997).

The only evidence of Late Pleistocene fluvial activity and deposition in the WSS is the Late Glacial Interstadial (LGI) OSL date of 14.7 ± 1.04 ka for W18 in MFQ. There is, however, evidence for deposits of this age elsewhere in Fenland, for example, 14.4 ± 0.6 ka at Maidcross Hill in Suffolk at the eastern margin of Fenland (Gibbard et al., 2021; Fig. 8). At Baston in the Welland catchment a ^{14}C date of $13\,474 \pm 300$ cal. yr BP and OSL date of 11.2 ± 1.5 ka (Briant et al., 2004d; Briant and Bateman, 2009) record accumulation spanning late in the LGI through to the Younger Dryas. The MIS 2–1 transition is recorded at Podehole by an OSL date of 10.5 ± 1.2 ka (Briant et al., 2005) on sediment infilling an ice-wedge cast and at Southorpe (Fig. 2) by a calibrated ^{14}C date of 11 165–9680 yr BP on peat (Scaiffe, 2004).

The time frame for the MIS 1 deposits at MFQ spans only about 4000 years, from late in the Atlantic climatic period to the current Sub-Atlantic climatic period (Fig. 8). Accumulation commenced late in the initial transgression of the north shore of The Wash and ended in the final transgression (Brew et al., 2015), embracing the three generations of roddons
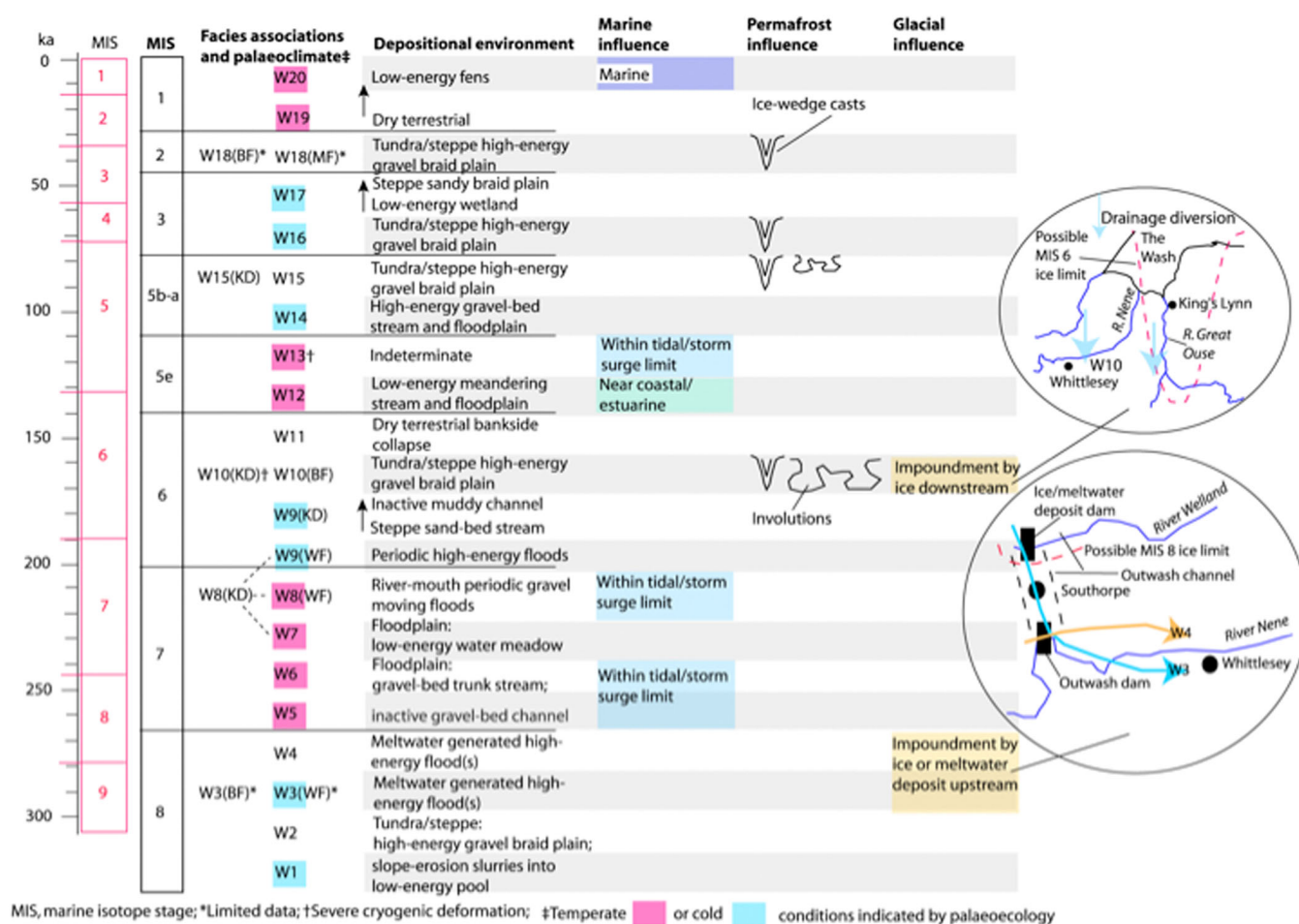

Figure 10. Summary diagram showing palaeoclimate indications and interpreted depositional environments for the facies associations identified within the Whittlesey sedimentary succession and their corresponding global climatic stages. Note that the base of W18 could be in MIS 3 and that of W16 could be in MIS 4. The inset diagrams are based on Langford (2018, 2025). There is no intent in this diagram to portray the proportion of time a facies association represents of its attributed corresponding MIS. Lisiecki and Raymo's (2005) stacked record from MIS 9 to MIS 1 (in red) with their interpreted timescale is also shown for comparison on the extreme left. [Color figure can be viewed at wileyonlinelibrary.com]

recorded in the MIS 1 deposits of Fenland (Horton, 1989) and accompanied by a rise in water level of 1.5 m in the last 2000 years of its 4000-year timespan. The long-established MIS 1 Fenland sequence of Lower Peat, Buttery/Fen Clay, Upper Peat and Warp/Upper Silt (Skertchley, 1877; Godwin, 1940) has been well documented for the area around Whittlesey. More recently, these stratigraphic terms have been superseded by the nomenclature Lower Peat, Barroway Drove Beds, Nordelph Peat and Terrington Beds (Table 1; Gallois, 1979). This sequence, however, is neither as complete (Waller, 1994) nor as simple (Horton, 1989) everywhere. The first two generations of roddons (Fig. 9) formed during the accumulation of the Barroway Drove Beds, whereas the third formed during the accumulation of the Terrington Beds (Horton, 1989). A robust geochronology for this MIS 1 Fenland sequence has been established by radiocarbon dates published in a number of studies (Horton, 1989; Waller, 1994, 2004; Knight and Brudenwell, 2020). Thus, the MIS 1 part of the WSS database could be extended and expanded upon from an extensive Fenland archaeological and geological literature.

Conclusion

This paper reports a robust geochronology for the late Middle Pleistocene to Holocene sedimentary succession at Whittlesey, eastern England. Twenty sedimentary facies associations have been established, 14 of which are constrained by luminescence, AAG or radiocarbon dating. Of the possible 39 upper and lower bracketing ages, 21 are dated numerically and in viable stratigraphic order. This provides a comprehensive and accurate record against which previous interpretations and palaeoenvironmental and palaeogeographical reconstructions can be assessed, as well as a framework within which ongoing and future work can be conducted. This publication is the culmination of 30 years of research attempting to unravel the complexity and geochronology of the WSS. Although reworking of earlier deposits is inevitable in a fluvial depositional environment, our research clearly demonstrates a robust approach to stratigraphical interpretation largely constrained by field relationships and age-estimate data using multiple techniques. Comprehensive multidisciplinary palaeoecological studies have identified potential reworked elements and established distinctive fossil assemblages that accord with the depositional environment. There remains, however, the potential to enhance understanding of the WSS and the potential to extend the depositional record to Fenland as a whole, as well as adopting this rationale for other stratigraphically complex successions; for example, Ebbsfleet (Wenban-Smith et al., 2020) and the pre-Anglian deposits of the north Norfolk coast (e.g. Preece et al., 2009, 2020). In light of this, the most important outcome therefore lies with others recognising the validity of the record and utilising it as a framework for future research. From our perspective, an important legacy would be the establishment of a comprehensive database that could be utilised to reconstruct different aspects of Fenland Quaternary history.

DATA AVAILABILITY STATEMENT

The data that support the findings of this study are published within the article, the supplementary information and previous publications.

Supporting information

Additional supporting information can be found in the online version of this article.
  Supplementary information:
  Supplementary information:

References

Aitken, M. (1985) *Thermoluminescence dating.* London: Academic Press.

Barlow, N., Long, A., Gehrels, W.R., Saher, M.H., Scaife, R.G., Davies, H.J. et al. (2017) Relative sea-level variability during the late Middle Pleistocene: new evidence from eastern England. *Quaternary Science Reviews*, 173, 20–39.

Bateman, M., Briant, R.M., Langford, H., Wheeler, L. & Whittaker, J. (2020) Determining the age of the late Middle Pleistocene marine March Gravel of eastern England. *Quaternary Newsletter*, 151, 13–20.

Bateman, M.D. (1999) The Ipswichian and Devensian Stages of the Quaternary Period in Britain. In: Langford, H.E., (compiler) *Cool Peterborough: Peterborough in the Ice Ages.* Peterborough: Langford Editorial Services. pp. 12–18.

Bateman, M.D., Boulter, C.H., Carr, A.S., Frederick, C.D., Peter, D. & Wilder, M. (2007) Detecting post-depositional sediment disturbance in sandy deposits using optical luminescence. *Quaternary Geochronology*, 2, 57–64.

Bateman, M.D. & Catt, J.A. (1996) An absolute chronology for the raised beach and associated deposits at Sewerby, East Yorkshire, England. *Journal of Quaternary Science*, 11, 389–395.

Bateman, M.D., Frederick, C.D., Jaiswal, M.K. & Singhvi, A.K. (2003) Investigations into the potential effects of pedoturbation on luminescence dating. *Quaternary Science Reviews*, 22, 1169–1176.

Bateman, M.D., Hitchens, S., Murton, J.B., Lee, J.R. & Gibbard, P.L. (2014) The evolution of periglacial patterned ground in East Anglia, UK. *Journal of Quaternary Science*, 29, 301–317.

BGS. (1980) *British Geological Survey (England and Wales): Ely Sheet 173, Solid and Drift Edition, 1:50,000 Series.* British Geological Survey, Keyworth, Nottingham.

BGS. (1984) *British Geological Survey (England and Wales): Peterborough Sheet 158, Solid and Drift Edition, 1:50,000 Series.* British Geological Survey, Keyworth, Nottingham.

BGS. (1995a) *British Geological Survey (England and Wales): Wisbech Sheet 159, Solid and Drift Edition, 1:50,000 Series.* British Geological Survey, Keyworth, Nottingham.

BGS. (1995b) *British Geological Survey (England and Wales): Ramsey Sheet 172, Solid and Drift Edition, 1:50,000 Provisional Series.* British Geological Survey, Keyworth, Nottingham.

Boreham, S., White, T.S., Bridgland, D.R., Howard, A.J. & White, M.J. (2010) The quaternary history of The Wash fluvial network, UK. *Proceedings of the Geologists' Association*, 121(4), 393–409.

Bowen, D.Q. Ed. (1999) *A revised correlation of quaternary deposits in the British Isles*. Bath, UK: Geological Society Publishing House.

Brew, D.S. (1997) The quaternary history of the subtidal central Wash, eastern England. *Journal of Quaternary Science*, 12, 131–141.

Brew, D.S., Horton, B.P., Evans, G., Innes, J.B. & Shennan, I. (2015) Holocene sea-level history and coastal evolution of the north-western Fenland, eastern England. *Proceedings of the Geologists' Association*, 126, 72–85.

Briant, R.M. & Bateman, M.D. (2009) Luminescence dating indicates radiocarbon age underestimation in Late Pleistocene fluvial deposits from eastern England. *Journal of Quaternary Science*, 24, 916–927.

Briant, R.M., Bateman, M.D., Coope, G. R. & Gibbard, P.L. (2005) Climatic control on quaternary fluvial sedimentology of a Fenland Basin river, England. *Sedimentology*, 52, 1397–1423.

Briant, R.M., Bates, M.R., Schwenninger, J.-L. & Wenban-Smith, F. (2006) An optically stimulated luminescence dated Middle to Late Pleistocene fluvial sequence from the western Solent Basin, southern England. *Journal of Quaternary Science*, 21, 507–523.

Briant, R.M., Brock, F., Demarchi, B., Langford, H.E., Penkman, K.E.H., Schreve, D.C. et al. (2018) Improving chronological control for environmental sequences from the last glacial period. *Quaternary Geochronology*, 43, 40–49.

Briant, R.M., Coope, G.R. & Bateman, M.D. (2004b) Pode Hole Quarry, Thorney (TF261033 to TF265033). In: Langford, H. E. & Briant, R. M. (Eds.) *Nene Valley*. Cambridge: Field Guide, Quaternary Research Association, pp. 130–144.

Briant, R.M., Coope, G.R., Bateman, M.D., Preece, R.C. & Griffiths, H.I. (2004a) Eye Quarry (TF237023 to TF240021). In: Langford, H.E. & Briant, R.M. (Eds.) *Nene Valley*. Cambridge: Field Guide, Quaternary Research Association, pp. 116–129.

Briant, R.M., Coope, G.R. & Gibbard, P.L. (2008) Limits to resolving catastrophic events in the Quaternary fluvial record: a case study from the Nene valley. In: Gallagher, K., Jones, S.J. & Wainwright, J. (Eds.) *Landscape evolution: denudation, climate and tectonics over different time and space scales*. Bath, UK: Geological Society Publishing House, pp. 79–104.

Briant, R.M., Coope, G.R., Preece, R.C., Keen, D.H., Boreham, S., Griffiths, H.I. et al. (2004d) Fluvial response to Late Devensian aridity, Baston, Lincolnshire, England. *Journal of Quaternary Science*, 19, 479–495.

Briant, R.M., Coope, G.R., Preece, R.C. & Gibbard, P.L. (2004c) The Upper Pleistocene deposits at deeping St James, Lincolnshire: evidence for Early Devensian fluvial sedimentation. *Quaternaire*, 15, 5–15.

Briant, R.M., Kilfeather, A.A., Parfitt, S., Penkman, K.E.H., Preece, R.C., Roe, H.M. et al. (2012) Integrated chronological control on an archaeologically significant Pleistocene river terrace sequence: the Thames–Medway, eastern Essex, England. *Proceedings of the Geologists' Association*, 123(1), 87–108.

Bridgland, D.R. (1994) *Quaternary of the Thames. Geological conservation review series, Joint Nature Conservation Committee.* London: Chapman & Hall.

Bridgland, D.R. (2010) The record from British Quaternary river systems within the context of global fluvial archives. *Journal of Quaternary Science*, 25(4), 433–446.

Bridgland, D.R., Howard, A.J., White, M.J., White, T.S. & Westaway, R. (2015) New insight into the quaternary evolution of the River Trent, UK. *Proceedings of the Geologists' Association*, 126, 466–479.

Bridgland, D.R., Keen, D.H. & Davey, N.D.W. (1991) The Pleistocene sequence in the Peterborough district: possible correlation with the deep-sea oxygen isotope record. In: Lewis, S.G., Whiteman, C.A. & Bridgland, D.R. *Central East Anglia and the Fen Basin, Field Guide.* London: Quaternary Research Association, pp. 209–212.

Brown, A.G., Basell, L.S. & Toms, P.S. (2015) A stacked Late Quaternary fluvio-periglacial sequence from the Axe valley, southern England with implications for landscape evolution and Palaeolithic archaeology. *Quaternary Science Reviews*, 116, 106–121.

Chancellor, G. & Langford, H. (1992) Two *Coelodonta antiquitatis* skulls found *in situ*: a preliminary report on River Nene First Terrace deposits. Peterborough. *Quaternary Newsletter*, 66, 18–21.

Church, M. (1974) Hydrology and permafrost with respect to North America, *Permafrost Hydrology: Proceedings of Workshop Seminar.* Ottawa: Canadian National Committee, International Hydrological Decade, Environment Canada, pp. 7–20.

Clark, C.D., Ely, J.C., Greenwood, S.L., Hughes, A.L.C., Meehan, R., Barr, I.D. et al. (2018) BRITICE Glacial Map, version 2: a map and GIS database of glacial landforms of the last British–Irish Ice Sheet. *Boreas*, 47, 11–27.

Cohen, K.M., Cartelle, V., Barnett, R., Busschers, F.S. & Barlow, N.L.M. (2022) Last interglacial sea-level data points from Northwest Europe. *Earth System Science Data*, 14, 2895–2937.

Colarossi, D., Duller, G.A.T., Roberts, H.M., Stirling, R.J. & Penkman, K.E.H. (2025) The effect of light exposure on the thermoluminescence signal from calcitic opercula. *Radiation Measurements*, 183, Article 107417.

Currant, A. & Jacobi, R. (2001) A formal mammalian biostratigraphy for the Late Pleistocene of Britain. *Quaternary Science Reviews*, 20, 1707–1716.

Dardis, G.F. (1984) Till facies associations in drumlins and some implications for their mode of formation. *Geografiska Annaler*, 67A, 13–22.

Davies, B.J., Bridgland, D.R., Roberts, D.H., Cofaigh, C.Ó., Pawley, S.M., Candy, I. et al. (2009) The age and stratigraphic context of the Easington Raised Beach, County Durham, UK. *Proceedings of the Geologists' Association*, 120(4), 183–198.

Demarchi, B. (2009) Geochronology of coastal prehistoric environments: a new closed system approach using amino acid racemisation. PhD thesis, University of York.

De Santis, V.D.S., Caldara, M.C., Torres, T.T., Ortiz, J.E.O. & Sánchez-Palencia, Y.S.P. (2018) A review of MIS 7 and MIS 5 terrace deposits along the Gulf of Taranto based on new stratigraphic and chronological data. *Italian Journal of Geosciences*, 137, 349–3680.

Duller, G.A.T., Kook, M., Stirling, R.J., Roberts, H.M. & Murray, A.S. (2015) Spatially-resolved thermoluminescence from snail opercula using an EMCCD. *Radiation Measurements*, 81, 157–162.

Duller, G.A.T. & Roberts, H.M. (2018) Seeing snails in a new light. *Elements*, 14(1), 39–43.

Duller, G.A.T. & Roberts, H.M. (2024) Chasing snails: Automating the processing of EMCCD images of luminescence from opercula. *Radiation Measurements*, 172, article 107084.

Evans, D.J., Roberts, D.H., Bateman, M.D., Ely, J., Medialdea, A., Burke, M.J. et al. (2019) A chronology for North Sea Lobe advance and recession on the Lincolnshire and Norfolk coasts during MIS 2 and 6. *Proceedings of the Geologists' Association*, 130(5), 523–540.

Fowler, G. (1933) Fenland waterways, past and present. *Proceedings of the Cambridge Antiquarian Society*, 33, 108–128.

Gallois, R.W. (1979) Geological investigations for the wash water storage scheme, *Institute of Geological Sciences Report, 78/19.* London: HMSO.

Geyh, M.A. & Müller, H. (2005) Numerical ^{230}Th/U dating and a palynological review of the Holsteinian/Hoxnian Interglacial. *Quaternary Science Reviews*, 24, 1861–1872.

Giaccio, B., Wagner, B., Zanchetta, G., Bertini, A., Cavinato, G.P., de Franco, R. et al. (2024) International Continental Scientific Drilling Program (ICDP) workshop on the Fucino paleolake project: the longest continuous terrestrial archive in the Mediterranean recording the last 5 Million years of Earth system history (MEME). *Scientific Drilling*, 33, 249–266.

Gibbard, P.L. (1985) *The Pleistocene history of the Middle Thames valley.* Cambridge: Cambridge University Press.

Gibbard, P.L., Bateman, M.D., Leathard, J. & West, R.G. (2021) Luminescence dating of a late Middle Pleistocene glacial advance in eastern England. *Netherlands Journal of Geosciences*, 100, e18.

Gibbard, P.L. & Hughes, P.D. (2021) Terrestrial stratigraphical division in the Quaternary and its correlation. *Journal of the Geological Society*, 178(2). Available from: https://doi.org/10.1144/jgs2020-134

Gibbard, P.L., Turner, C. & West, R.G. (2012) The Bytham river reconsidered. *Quaternary International*, 292, 15–32.

Gibbard, P.L., West, R.G. & Hughes, P.D. (2018) Pleistocene glaciation of Fenland, England, and its implications for evolution of the region. *Royal Society Open Science*, 5, 170736.

Gibson, S.M., Bateman, M.D., Murton, J.B., Barrows, T.T., Fifield, L.K. & Gibbard, P.L. (2022) Timing and dynamics of Late Wolstonian Substage 'Moreton Stadial' (MIS 6) glaciation in the English West

Midlands, UK. *Royal Society Open Science*, 9(6), 220312. Available from: https://doi.org/10.1098/rsos.220312

Godwin, H. (1940) Studies of the post-glacial history of British vegetation III. Fenland pollen diagrams IV. Post-glacial changes of relative land and sea-level in the English Fenland. *Philosophical Transactions of the Royal Society of London, Series B*, 230, 239–303.

Green, C.P., Coope, G.R., Jones, R.L., Keen, D.H., Bowen, D.Q., Currant, A.P. et al. (1996) Pleistocene deposits at Stoke Goldington, in the valley of the Great Ouse, UK. *Journal of Quaternary Science*, 11, 59–87.

Guérin, G., Mercier, N. & Adamiec, G. (2011) Dose-rate conversion factors: update. *Ancient TL*, 29, 5–8.

Hatch, M., Davis, R.J., Lewis, S.G., Ashton, N., Briant, R.M. & Lukas, S. (2017) The stratigraphy and chronology of the fluvial sediments at Warsash, UK: implications for the Palaeolithic archaeology of the River Test. *Proceedings of the Geologists' Association*, 128, 198–221.

Hollin, J.T. (1996) Review. *Arctic and Alpine Research*, 28(4), 529–531.

Holmes, J.A. & De Deckker, P. (2017) Trace-element and stable-isotope composition of the *Cyprideis torosa* (Crustacea, Ostracoda) shell. *Journal of Micropalaeontology*, 36, 38–49.

Holyoak, D.T. & Seddon, M.B. (1984) Devensian and Flandrian fossilerous deposits in the Nene valley, central England. *Mercian Geologist*, 9(3), 127–150.

Horne, D.J. (2007) A mutual temperature range method for Quaternary palaeoclimatic analysis using European nonmarine Ostracoda. *Quaternary Science Reviews*, 26, 1398–1415.

Horne, D.J., Ashton, N., Benardout, G., Brooks, S.J., Coope, G.R., Holmes, J.A. et al. (2023) A terrestrial record of climate variation during MIS 11 through multi-proxy palaeotemperature reconstructions from Hoxne, UK. *Quaternary Research*, 111, 21–52.

Horne, D.J., Curry, B.B. & Mesquita-Joanes, F. (2012) Mutual climatic range methods for Quaternary ostracods. In: Horne, D.J., Holmes, J.A., Rodriguez-Lazaro, J. & Viehberg, F.A. (Eds.) *Ostracoda as Proxies for Quaternary Climate Change: Developments in Quaternary Science 17*. Amsterdam: Elsevier, pp. 65–84.

Horne, D.J. & Mezquita, F. (2008) Palaeoclimatic applications of large databases: developing and testing methods of palaeotemperature reconstruction using nonmarine ostracods. *Senckenbergiana Lethaea*, 88, 93–112.

Horton, A. (1989) Geology of the Peterborough district, *Memoir of the British Geological Survey, Sheet 158*. London: HMSO, p. 44.

Horton, A., Keen, D.H., Field, M.H., Robinson, J.E., Coope, G.R., Currant, A.P. et al. (1992) The Hoxnian Interglacial deposits at Woodston, Peterborough. *Philosophical Transactions of the Royal Society of London. Series B: Biological Sciences*, 338, 131–164.

Howard, A.J., Bridgland, D., Knight, D., McNabb, J., Rose, J., Schreve, D. et al. (2007) The British Pleistocene fluvial archive: East Midlands drainage evolution and human occupation in the context of the British and NW European record. *Quaternary Science Reviews*, 26, 2724–2737.

Jones, A.P. (1999) Background to sedimentary facies. In: Jones, A.P., Tucker, M.E. & Hart, J.K. *The description and analysis of quaternary stratigraphic field sections*. London: Quaternary Research Association, pp. 5–26.

Kaufman, D., McKay, N., Routson, C., Erb, M., Davis, B., Heiri, O. et al. (2020) A global database of Holocene paleotemperature records. *Scientific Data*, 7, 115–149.

Keen, D.H., Bateman, M.D., Coope, G.R., Field, M.H., Langford, H.E., Merry, J.S. et al. (1999) Sedimentology, palaeoecology and geochronology of Last Interglacial deposits from Deeping St James, Lincolnshire, England. *Journal of Quaternary Science*, 14, 411–436.

Kerney, M.P. (1999) *Atlas of the land and freshwater molluscs of Britain and Ireland*. Colchester: Harley Books.

Knight, M., Ballantyne, R., Brudenell, M., Cooper, A., Gibson, D. & Robinson Zeki, I. (2024) *Must Farm Pile-dwelling Settlement: Landscape, Architecture and Occupation*, 1. Cambridge: McDonald Institute for Archaeological Research.

Knight, M. & Brudenwell, M. (2020) *Pattern and process: landscape prehistories from Whittlesey Brick Pits: the King's Dyke and Bradley Fen Excavations 1998–2004*. Cambridge: McDonald Institute for Archaeological Research.

Krahn, K.J., Tucci, M., Urban, B., Pilgrim, J., Frenzel, P., Soulié-Märsche, I. et al. (2021) Aquatic and terrestrial proxy evidence for Middle Pleistocene palaeolake and lake-shore development at two Lower Palaeolithic sites of Schöningen, Germany. *Boreas*, 50, 723–745.

Krahn, K.J., Urban, B., Pinkerneil, S., Horne, D.J., Tucci, M., Koutsodendris, A. et al. (2024) Temperature and palaeolake evolution during a Middle Pleistocene interglacial–glacial transition at the Palaeolithic locality of Schöningen, Germany. *Boreas*, 53, 504–524.

Lamothe, M., Balescu, S. & Auclair, M. (1994) Natural IRSL intensities and apparent luminescence ages of single feldspar grains extracted from partially bleached sediments. *Radiation Measurements*, 23, 555–561.

Langford, H.E. (1999) Sedimentological, palaeogeographical and stratigraphical aspects of the Middle Pleistocene geology of the Peterborough area, eastern England. PhD thesis, Anglia Polytechnic University, Cambridge.

Langford, H.E. (2002) Middle to Late Pleistocene deposits at Whittlesey, eastern England. *Quaternary Newsletter*, 97, 46–49.

Langford, H.E. (2004) Middle Pleistocene deposits at Stanground (Peterborough) and March, eastern England: a discussion based on new evidence. *Proceedings of the Geologists' Association*, 115, 91–95.

Langford, H.E. (2011) New sediment magnetic data from Anglian (Middle Pleistocene) glacial deposits in the Peterborough area, eastern England: a comparison with data from Norfolk and Suffolk. *Bulletin of the Geological Society of Norfolk*, 61, 3–22.

Langford, H.E. (2018) Drainage network reorganization affecting the Nene and Welland catchments of eastern England as a result of a late Middle Pleistocene glacial advance. *The Depositional Record*, 4, 177–201.

Langford, H.E. (2025) Comments on 'Late Middle Pleistocene Wolstonian Stage (MIS 6) glaciation in lowland Britain and its North Sea regional equivalents—a review. *Boreas*. Available from: https://doi.org/10.1111/bor.70011

Langford, H.E. & Briant, R.M. Eds. (2004) *Nene valley*. Cambridge: Field Guide, Quaternary Research Association.

Langford, H.E., Bateman, M.D., Boreham, S., Coope, G.R., Fletcher, W., Green, C.P. et al. (2004b) Funtham's Lane East. In: Langford, H.E. & Briant, R.M. (Eds.) *Nene Valley*. Cambridge: Field Guide, Quaternary Research Association, pp. 69–106.

Langford, H.E., Bateman, M.D., Boreham, S., Knudsen, K.-L., Merry, J. & Penney, D. (2004a) King's Dyke. In: Langford, H.E. & Briant, R.M. (Eds.) *Nene Valley*. Cambridge: Field Guide, Quaternary Research Association, pp. 174–194.

Langford, H.E., Bateman, M.D., BriantHorne, D.J., Knudsen, K.-L., Penkman, K.E.H. et al. (in press) New age-estimate data and implications for marine isotope stage 7 and 5e sea levels in Fenland, Eastern England. *Journal of Quaternary Science*. Available from: https://doi.org/10.1002/jqs.70025

Langford, H.E., Bateman, M.D., Penkman, K.E.H., Boreham, S., Briant, R.M., Coope, G.R. et al. (2007) Age-estimate evidence for Middle–Late Pleistocene aggradation of River Nene 1st Terrace deposits at Whittlesey, eastern England. *Proceedings of the Geologists' Association*, 118, 283–300.

Langford, H.E., Boreham, S., Briant, R.M., Coope, G.R., Horne, D.J., Schreve, D.S. et al. (2014b) Middle to Late Pleistocene palaeoecological reconstructions and palaeotemperature estimates for cold/cool stage deposits at Whittlesey, eastern England. *Quaternary International*, 341, 6–26.

Langford, H.E., Boreham, S., Briant, R.M., Coope, G.R., Horne, D.J., Penkman, K.E.H. et al. (2017) Evidence for the early onset of the Ipswichian thermal optimum: palaeoecology of Last Interglacial deposits at Whittlesey, eastern England. *Journal of the Geological Society*, 174, 988–1003.

Langford, H.E., Boreham, S., Coope, G.R., Fletcher, W., Keen, D.H., Mighall, T. et al. (2014a) Palaeoecology of a late MIS 7 interglacial deposit from eastern England. *Quaternary International*, 341, 27–45.

Langford, H.E., Boreham, S., Merry, J.S., Rolfe, C. & Schreve, D.C. (2004c) Channels C and D at Bradley Fen. In: Langford, H.E. & Briant, R.M. (Eds.) *Nene Valley*. Cambridge: Field Guide, Quaternary Research Association, pp. 107–115.

Langford, H.E., Griffiths, H., Horne, D.J., KeenPenkman, K.E.H. (2020) Age-estimate evidence for a complex Middle to Late Pleistocene fluvial terrace aggradation spanning more than a 100-kyr

interglacial–glacial cycle at Sutton Cross, eastern England. *Proceedings of the Geologists' Association*, 131, 758–777.

Lauterbach, S., Neumann, F.H., Tjallingii, R. & Brauer, A. (2024) Re-investigation of the Bispingen palaeolake sediment succession (northern Germany) reveals that the Last Interglacial (Eemian) in northern-central Europe lasted at least ~15 000 years. *Boreas*, 53, 243–261.

Lee, J.R., Bateman, M.D. & Hitchens, S. (2015) Pleistocene glacial and periglacial geology. In: Lee, J.R., Woods, M.A. & Moorlock, B.S.P. *British Regional Geology: East Anglia*, 5. Keyworth, Nottingham: British Geological Survey, pp. 146–172.

Lewis, S.G., Ashton, N., Davis, R., Hatch, M., Hoare, P.G., Voinchet, P. et al. (2021) A revised terrace stratigraphy and chronology for the early Middle Pleistocene Bytham river in the Breckland of East Anglia, UK. *Quaternary Science Reviews*, 269, 107113.

Lisiecki, L.E. & Raymo, M.E. (2005) A Pliocene–Pleistocene stack of 57 globally distributed benthic δ^{18}O records. *Paleoceanography*, 20, PA1003. Available from: https://doi.org/10.1029/2004PA001071

Macfadyen, W.A. (1933) The Foraminifera of the Fenland Clays at St. Germans, near King's Lynn. *Geological Magazine*, 70, 182–191.

Maddy, D. (1999) English Midlands. In: Bowen, D.Q. (Ed.) *A Revised Correlation of Quaternary Deposits in the British Isles*. Bath, UK: Geological Society Publishing House.

Maddy, D., Keen, D.H., Bridgland, D.R. & Green, C.P. (1991) A revised model for the Pleistocene development of the River Avon, Warwickshire. *Journal of the Geological Society*, 148(3), 473–484.

Meijer, T. & Cleveringa, P. (2009) Aminostratigraphy of Middle and Late Pleistocene deposits in The Netherlands and the southern part of the North Sea Basin. *Global and Planetary Change*, 68, 326–345.

Miall, A.D. (1977) A review of the braided river depositional environment. *Earth-science Reviews*, 13, 1–62.

Miller, G.H. & Mangerud, J. (1985) Aminostratigraphy of European marine interglacial deposits. *Quaternary Science Reviews*, 4, 215–278.

Mills, M., Schreve, D., Middleton, O. & Sandom, C.J. (2024) Going back for the future: incorporating Pleistocene fossil records of saiga antelope into habitat suitability models. *Journal of Biogeography*, 51, 1351–1364.

Morgan, A. (1969) A Pleistocene fauna and flora from Great Billing, Northamptonshire, England. *Opuscula Entomologica, Lund*, 34(1–2), 109–129.

Murray, A.S. & Funder, S. (2003) Optically stimulated luminescence dating of a Danish Eemian coastal marine deposit: a test of accuracy. *Quaternary Science Reviews*, 22, 1177–1183.

Murray, A.S. & Wintle, A.G. (2000) Luminescence dating of quartz using an improved single-aliquot regenerative-dose protocol. *Radiation Measurements*, 32, 57–73.

Murray, A.S. & Wintle, A.G. (2003) The single aliquot regenerative dose protocol: potential for improvements in reliability. *Radiation Measurements*, 37, 377–381.

Murton, J.B., Bowen, D.Q., Candy, I., Catt, J.A., Currant, A., Evans, J.G. et al. (2015) Middle and Late Pleistocene environmental history of the Marsworth area, south-central England. *Proceedings of the Geologists' Association*, 126(1), 18–49.

Olley, J.M., De Deckker, P., Roberts, R.G., Fifield, L.K., Yoshida, H. & Hancock, G. (2004) Optical dating of deep-sea sediments using single grains of quartz: a comparison with radiocarbon. *Sedimentary Geology*, 169, 175–189.

Ortiz, J.E., Torres, T. & Pérez-González, A. (2013) Amino acid racemization in four species of ostracodes: taxonomic, environmental, and microstructural controls. *Quaternary Geochronology*, 16, 129–143.

Pearce, E.A., Mazier, F., Davison, C.W., Baines, O., Czyżewski, S., Fyfe, R. et al. (2025) Beyond the closed-forest paradigm: cross-scale vegetation structure in temperate Europe before the late-Quaternary megafauna extinctions. *Earth History and Biodiversity*, 3, 100022. Available from: https://doi.org/10.1016/j.hisbio.2025.100022

Penkman, K.E.H. (2005) Amino acid geochronology: a closed system approach to test and refine the UK model. Unpublished PhD thesis, University of Newcastle.

Penkman, K.E.H., Preece, R.C., Bridgland, D.R., Keen, D.H., Meijer, T., Parfitt, S.A. et al. (2011) A chronological framework for the British Quaternary based on *Bithynia* opercula. *Nature*, 476, 446–449.

Penkman, K.E.H., Preece, R.C., Bridgland, D.R., Keen, D.H., Meijer, T., Parfitt, S.A. et al. (2013) An aminostratigraphy for the British

Quaternary based on *Bithynia* opercula. *Quaternary Science Reviews*, 61, 111–134.

Preece, R., Meijer, T., Penkman, K., Demarchi, B., Mayhew, D. & Parfitt, S. (2020) The palaeontology and dating of the 'Weybourne Crag', an important marker horizon in the Early Pleistocene of the southern North Sea basin. *Quaternary Science Reviews*, 236, article 106177.

Preece, R.C., Parfitt, S.A., Coope, G.R., Penkman, K.E.H., Ponel, P. & Whittaker, J.E. (2009) Biostratigraphic and aminostratigraphic constraints on the age of the Middle Pleistocene glacial succession in north Norfolk, UK. *Journal of Quaternary Science*, 24, 557–580.

Prescott, J.R. & Hutton, J.T. (1994) Cosmic-ray contributions to dose-rates for luminescence and ESR dating—large depths and long-term time variations. *Radiation Measurements*, 23, 497–500.

Railsback, L.B., Gibbard, P.L., Head, M.J., Voarintsoa, N.R.G. & Toucanne, S. (2015) An optimized scheme of lettered marine isotope substages for the last 1.0 million years, and the climatostratigraphic nature of isotope stages and substages. *Quaternary Science Reviews*, 111, 94–106.

Reading, H.G. (1996) *Sedimentary environments: processes, facies and stratigraphy*, 3rd edn. Oxford: Blackwell Science.

Rhodes, E.J. (2015) Dating sediments using potassium feldspar single-grain IRSL: initial methodological considerations. *Quaternary International*, 362, 14–22.

Rigterink, S., Krahn, K.J., Kotrys, B., Urban, B., Heiri, O., Turner, F. et al. (2024) Summer temperatures from the Middle Pleistocene site Schöningen 13 II, northern Germany, determined from subfossil chironomid assemblages. *Boreas*, 53, 525–542.

Roberts, D.H., Evans, D.J.A., Callard, S.L., Clark, C.D., Bateman, M.D., Medialdea, A. et al. (2018) Ice marginal dynamics of the last British-Irish Ice Sheet in the southern North Sea: ice limits, timing and the influence of the Dogger Bank. *Quaternary Science Reviews*, 198, 181–207.

Rose, J. (2009) Early and Middle Pleistocene landscapes of eastern England. *Proceedings of the Geologists' Association*, 120, 3–33.

Rose, J. (2015) Pleistocene fluvial deposits and soils. In: Lee, J.R., Woods, M.A. & Moorlock, B.S.P. (Eds.) *British Regional Geology: East Anglia*, 5th edn. Keyworth, Nottingham: British Geological Survey. pp. 130–145.

Scaife, R. (2004) Southorpe. In: Langford, H.E. & Briant, R.M. (Eds.) *Nene Valley*. Cambridge: Field Guide, Quaternary Research Association. pp. 149–154.

Schaumann, R.M., Capperucci, R.M., Bungenstock, F., McCann, T., Enters, D., Wehrmann, A. et al. (2021) The Middle Pleistocene to early Holocene subsurface geology of the Norderney tidal basin: new insights from core data and high resolution sub-bottom profiling (Central Wadden Sea, southern North Sea). *Netherlands Journal of Geosciences*, 100, e15.

Schreve, D.C. (2001) Mammalian evidence from Middle Pleistocene fluvial sequences for complex environmental change at the oxygen isotope substage level. *Quaternary International*, 79, 65–74.

Sier, M.J., Peeters, J., Dekkers, M.J., Parés, J.M., Chang, L., Busschers, F.S. et al. (2015) The Blake Event recorded near the Eemian type locality—a diachronic onset of the Eemian in Europe. *Quaternary Geochronology*, 28, 12–28.

Skertchly, S.B.J. (1877) *The Geology of the Fenland. Memoir of the Geological Survey of Great Britain*. London: Her Majesty's Stationery Office.

Smith, D.M., Zalasiewicz, J.A., Williams, M., Wilkinson, I.P., Scarborough, J.J., Knight, M. et al. (2012) The anatomy of a Fenland roddon: sedimentation and environmental change in a lowland Holocene tidal creek environment. *Proceedings of the Yorkshire Geological Society*, 59(2), 145–159.

Sparks, B.W. & West, R.G. (1970) Late Pleistocene deposits at Wretton, Norfolk. I. Ipswichian Interglacial deposits. *Philosophical Transactions of the Royal Society of London, Series B: Biological Sciences*, 258(818), 1–30.

Stephan, H.-J. (2014) Climato-stratigraphic subdivision of the Pleistocene in Schleswig-Holstein, Germany and adjoining areas. *E&G Quaternary Science Journal*, 63(1), 3–18.

Straw, A. (2000) Some observations on 'Eastern England' in *A Revised Correlation of Quaternary deposits in the British Isles* (Ed. D.Q.Bowen, 1999). *Quaternary Newsletter*, 91, 2–6.

Straw, A. (2011) The Saale glaciation of eastern England. *Quaternary Newsletter*, 123, 28–35.

Taylor, J.H. (1963) The geology of the country around Kettering, Corby and Oundle, *Memoir of the Geological Survey of Great Britain*. London: HMSO.

Tye, G.J., Sherriff, J., Candy, I., Coxon, P., Palmer, A., McClymont, E.L. et al. (2016) The δ¹⁸O stratigraphy of the Hoxnian lacustrine sequence at Marks Tey, Essex, UK: implications for the climatic structure of MIS 11 in Britain. *Journal of Quaternary Science*, 31, 75–92.

Urban, B. (1995) Palynological evidence of younger Middle Pleistocene Interglacials (Holsteinian, Reinsdorf, Schöningen) in the Schöningen open cast lignite mine (eastern Lower Saxony/ Germany). *Mededelingen Rijks Geologische Dienst*, 52, 175–186.

Waller, M.P. (1994) The Fenland Project, Number 9, Flandrian environmental change in Fenland. Monograph 70, East Anglian Archaeology, Cambridge.

Waller, M.P. (2004) The Holocene deposits of Holme Fen and Whittlesey Mere: a reappraisal. In: Langford, H.E. & Briant, R.M. (Eds.) *Nene Valley*. Cambridge: Field Guide, Quaternary Research Association. pp. 63–69.

Wenban-Smith, F., Stafford, E., Bates, M. & Parfitt, A. (2020) *Prehistoric Ebbsfleet: excavations and research in advance of High Speed 1 and South Thameside Development Route 4, 1989–2003*. Monograph 7, Oxford Wessex Archaeology, Salisbury.

West, R.G. (1991) *Pleistocene palaeoecology of central Norfolk: a study of environments through time*. Cambridge: Cambridge University Press.

West, R.G. (1993) On the history of the Late Devensian Lake Sparks in southern Fenland, Cambridgeshire, England. *Journal of Quaternary Science*, 8, 217–234.

West, R.G., Andrew, R., Catt, J.A., Hart, C.P., Hollin, J.T., Knudsen, K.L. et al. (1999) Late and Middle Pleistocene deposits at Somersham, Cambridgeshire, UK: a model for reconstructing fluvial/estuarine depositional environments. *Quaternary Science Reviews*, 18(11), 1247–1314.

West, R.G., Peglar, S.M., Pettit, M.E. & Preece, R.C. (1995) Late Pleistocene deposits at Block Fen, Cambridgeshire, England. *Journal of Quaternary Science*, 10, 285–310.

Westaway, R. (2009) Calibration of decomposition of serine to alanine in *Bithynia* opercula as a quantitative dating technique for Middle and Late Pleistocene sites in Britain. *Quaternary Geochronology*, 4, 241–259.

Westaway, R. (2010) Implications of recent research for the timing and extent of Saalian glaciation of eastern and central England. *Quaternary Newsletter*, 121, 3–23.

Westerhold, T., Agnini, C., Anagnostou, E., Hilgen, F., Hönisch, B., Meckler, A.N. et al. (2024) Timing is everything. *Paleoceanography and Paleoclimatology*, 39, e2024PA004932.

White, T.S., Bridgland, D.R., Westaway, R., Howard, A.J. & White, M.J. (2010) Evidence from the Trent terrace archive, Lincolnshire, UK, for lowland glaciation of Britain during the Middle and Late Pleistocene. *Proceedings of the Geologists' Association*, 121, 141–153. Available from: https://doi.org/10.1016/j.pgeola.2010.05.001

White, T.S., Bridgland, D.R., Westaway, R. & Straw, A. (2017) Evidence for late Middle Pleistocene glaciation of the British margin of the southern North Sea. *Journal of Quaternary Science*, 32(2), 261–275.

Appendix: Potential MIS 7 substage stratigraphy

This appendix explores multiple stratigraphical considerations that emerge from possible scenarios that arise from recent research of the Whittlesey sedimentary succession (WSS). Table A1 presents the constraints on those scenarios according to that research. Considering first the possibility of a MIS 7 age for the dated material from the organic mud beds at the top of W3(WF) (Fig. 4) indicated by the opercula AAG (Fig. 7(a), (b)). As the palaeoecology of the fossil assemblage of the organic mud beds indicates accumulation under cool/cold conditions, in this scenario, the dated opercula are likely to have been reworked from either MIS 7e or 7c. There is no evidence of the exotic molluscan species prevalent in channel B (W5 and W6; *Belgrandia marginata*, *Theodoxus danubialis* and *Corbicula* cf. *fluminalis*), so reworking of earlier temperate material other than that represented by channel B is suggested. Channel B, however, is post-dated by W7 and W8(WF), both dated by opercula AAG to MIS 7, and both containing distinctive fully temperate faunal assemblages. Considering the possibility that both W7 and W8(WF) represent the same temperate substage of MIS 7 restricts the *dated material* in the organic mud beds to 7e, the organic mud beds to 7d, channel B to 7c and W7 and W8(WF) to 7a. This in turn restricts the weathering phase that post-dates channel B, but pre-dates W7 and W8(WF), to between 7c and 7a, and the secondary Ca cementation at the top of W3(BF) to 7a. Intriguingly, a reworked mud clast at the base of W8 (WF) (OMC, Fig. 4; sample 49, Tables S9 and S10) has a restricted fossil assemblage that differs slightly to that from the organic mud beds of W3(WF) (Langford et al., 2007, 2014a), with the ostracod fauna also indicating cool/cold conditions (unpublished data), thus raising the possibility of representing MIS 7b.

Table A1. Potential stratigraphical interpretation at climatic substage level for the MIS 7 sequence in the Whittlesey sedimentary succession.

Potential stratigraphical interpretation	Marine isotope substage				
	7e	7d	7c	7b	7a
Age of dated material in organic mud beds at the top of W3(WF), if attributable to MIS 7	■		■		
Age of organic mud beds at the top of W3(WF), if attributable to MIS 7		■		■	
Late temperate woodland pollen restricts the age of channel B to (because W7 and W8(WF) have evidence of fully interglacial conditions and demonstrably post-date W5 and W6)	■		■		
Formation of FH in WFQ restricted to	■	■	■	■	■
Age of W7 restricted to (because FH restricted downward and eastward percolation of Ca-rich water in WFQ)				■	■
Formation of CH in BFQ restricted to (as it results from westward percolation of Ca-rich water from W7)			■		■
Age of W8(WF) restricted to (because of the presence of RFH and W7? at base of W8(WF))			■		■
Age of W8(KD), if equivalent to W8(WF), restricted to			■		■
Age of reworked material in W8(KD) restricted to	■			■	

Bearing in mind that W8(WF) records the first influx of marine (rather than just brackish as in channel B) fauna within the MIS 7 sequence in WFQ and BFQ (between about −2 and +0.5 m OD) and that W7 records accumulation under high water table conditions (between about +1 and +2.5 m OD), how likely is it that both W7 and W8(WF) date to MIS 7a? In the scenario where W7 pre-dates W8(WF), habitats suitable for *B. marginata* and *Psychrodomus olivaceus* were available at about +2 m OD and at about −2 m OD following downcutting, which paradoxically heralded an influx of marine microfauna and subsequent cessation upward of habitats suitable for *B. marginata* and *P. olivaceus*. Whereas in the scenario where W8(WF) pre-dates W7, there is no upward indication of progressive transgression in W8 (WF) nor accompanying the rise in water table necessary for the accumulation of W7. Rather, there is upward cessation of habitats suitable for *B. marginata* and *P. olivaceus* (above −2 m OD) and a change to fully fluvial conditions above +0.5 m OD, superseded by low-energy floodplain conditions prior to a fall in the water table and the reappearance of *B. marginata* and *P. olivaceus*.

Neither of these scenarios for both W7 and W8(WF) dating to MIS 7a seems as plausible as them representing separate temperate substages, with the *B. marginata* and *P. olivaceus* of sample FC2b at the base of W8(WF) being reworked from the top of W7. Thus, with both undoubtedly post-dating channel B, W5 and W6 would represent 7e, W7 substage 7c and W8(WF) substage 7a. The absence of exotic shell material characteristic of channel B in the organic mud beds at the top of W3(WF) in this circumstance implies an MIS 9 age for the *dated material* and an MIS 8 age for W3(WF); the possibility of the OMC at the base of W8(WF) representing 7b also remains, but 7 d cannot be ruled out.

Beyond the WSS, there are estuarine deposits up to +2.5 m OD at Northam Pit (Eye; Figs. 1 and 2) with a maximum age of MIS 7c (Bateman et al., 2020) that could correspond to marine-influenced deposits of W5–W8. There is, however, no direct evidence of deposits within the WSS directly related to the Northam Pit transgression. Neither is there direct evidence of MIS 7 outer-estuarine–marine conditions more proximal to the WSS than the Northam Pit estuarine deposits (Langford et al., in press). Channel B deposits from about −1 to +2 m OD represent a distal upstream location with possible direct connections to the sea, the lower part of W8(WF) from about −2 to +0.5 m OD could represent a distal inner estuary environment and W8(KD) deposits from about +3.4 to +3.9 m OD represent a shallow pool in a fluviatile setting, with the fauna being reworked from earlier MIS 7 deposits. In terms of age, the estuarine deposits at Northam Pit could correspond to any of the W5–W8 deposits in the scenario where the *dated material* in the organic mud beds at the top of W3(WF) was MIS 7 in age, but only to W7 or W8 otherwise. In terms of altitude and concomitant high water table conditions, the closest correspondence is with W7 and W8(KD).